

Computationally Efficient Signal Detection with Unknown Bandwidths

Ali Rasteh, Sundeep Rangan

Abstract—Signal detection in environments with unknown signal bandwidth and time intervals is a fundamental problem in adversarial and spectrum-sharing scenarios. This paper addresses the problem of detecting signals occupying unknown degrees of freedom from non-coherent power measurements, where the signal is constrained to an interval in one dimension or a hypercube in multiple dimensions. A Generalized Likelihood Ratio Test (GLRT) is derived, resulting in a straightforward metric involving normalized average signal energy for each candidate signal set. We present bounds on false alarm and missed detection probabilities, demonstrating their dependence on signal-to-noise ratios (SNRs) and signal set sizes. To overcome the inherent computational complexity of exhaustive searches, we propose a computationally efficient binary search method, reducing the complexity from $O(N^2)$ to $O(N)$ for one-dimensional cases. Simulations indicate that the method maintains performance near exhaustive searches and achieves asymptotic consistency, with interval-of-overlap converging to one under constant SNR as measurement size increases. The simulation studies also demonstrate superior performance and reduced complexity compared to contemporary neural network-based approaches, specifically outperforming custom-trained U-Net models in spectrum detection tasks.

Index Terms—Spectrum Sensing, Efficient Spectrum Detection, Cognitive Radio, Maximum Likelihood Estimation (MLE), Binary Hypothesis Testing, Neural Networks for Signal Detection

I. INTRODUCTION

SIGNAL detection is a fundamental problem in various fields, such as communications, radar, and biomedical engineering [1]–[4]. In many problems, the time interval and bandwidth that the signal occupies are not known *a priori*. In these cases, signal detection must be performed in parallel with time and bandwidth estimation. This situation arises most obviously in adversarial scenarios where an interfering signal can have an arbitrary center frequency, bandwidth, and time interval. The situation may also arise in future spectrum co-existence scenarios where multiple services use arbitrary bandwidths or frequency hopping for flexibility [2], [5]–[7]. Signal detection is also potentially important in emerging systems in the upper mid-band for co-existence between disparate systems [8], [9].

In this paper, we consider the general problem of detecting a signal from a set of non-coherent power measurements. The signal, when present, occupies an unknown set S of the degrees of freedom. Classical frequency-domain energy

detectors (FD-ED) methods typically assume a fixed sensing bandwidth or rely on known band structures (e.g., WiFi channels, LTE sub-bands). In contrast, our method explicitly addresses the case where the signal may occupy an arbitrary and unknown interval in the frequency (or, more generally, multi-dimensional) domain, under which FD-ED proves inadequate. One power measurement is made on each degree of freedom, and the set of power measurements is modeled as exponential random variables with a higher mean on the degrees of freedom in S . While the exponential distribution of single-bin energies under additive white Gaussian noise (AWGN) is well established, the novelty of this work lies in addressing the unknown signal structure and developing the associated search and detection methods. We consider both one-dimensional and multi-dimensional search problems, where the signal set S consists of an unknown interval or hypercube within the measurement space. The dimensions of the measurement space could be frequency, time, angle of arrival, etc. The primary focus of this work is on non-cooperative networks, where users independently sense the spectrum using the proposed method. Nevertheless, the approach is flexible and can also be applied in cooperative scenarios where users share spectrum sensing information. The proposed method is applicable to both single-antenna and multi-antenna systems. Since the core objective is to address the detection problem—determining the presence or absence of signals at the initial stage of the processing pipeline—a single antenna is sufficient to implement our method. However, employing multiple antennas can further improve the SNR and enhance detection performance. Importantly, the system model does not impose any coherence constraints; however, an essential calibration phase is requisite for the accurate estimation of the noise power.

Existing spectrum sensing research spans a wide range of techniques, from classical energy detection – effective when little signal information is available – to more sophisticated approaches such as matched filtering, feature-based detection, eigenvalue methods, and numerous machine learning and deep learning–based classifiers. Although advanced detectors can offer strong performance, they often depend on prior knowledge of signal structure or incur significant computational costs, making them less suitable for real-time, resource-constrained environments. Frequency-domain and transform-based methods further improve detection but typically assume a known band structure or operate under wideband, high-rate sampling constraints, while sub-Nyquist strategies introduce their own complexities. Overall, while many algorithms exist, they either rely on restrictive assumptions, demand substantial

A. Rasteh and S. Rangan are with New York University, Brooklyn, NY (e-mail: ar7655, srangan@nyu.edu). Their work is supported in part by NSF grants 1952180, 2133662, 2236097, 2148293, and 1925079, the DARPA Prowess program, the NTIA and industrial affiliates, of NYU Wireless.

computation, or fail to address practical constraints. These limitations motivate our work, which aims to provide an efficient, low-complexity detection method that requires minimal prior signal information and remains effective even when bandwidth and carrier frequency are unknown.

Our contributions are as follows.

- *Derivation of the Generalized Likelihood Ratio Test (GLRT)*: We derive a simple GLRT [10], [11] for the detection problem. For each possible candidate signal set S that the signal can occupy, it is shown that the GLRT can be computed from a simple metric of the average signal energy on the interval S , normalized by the number of degrees of freedom in S . The GLRT then maximizes the metric over the sets.
- *Receiver Operating Characteristic*: Bounds are provided for both the false alarm and missed detection probabilities, with the missed detection probability depending on the size of the signal set and the signal-to-noise ratio (SNR).
- *Computationally efficient binary search*: A key challenge in the GLRT is that all signal sets S must be searched. For a one-dimensional problem with N degrees of freedom, the search over all intervals will have a complexity of $O(N^2)$. We present a binary search method with a complexity of $O(N)$. This efficiency is particularly critical in wideband scenarios where FD-ED would either miss signals or require prohibitively high sampling overhead.
- *Asymptotic consistency of binary search*: Our main theoretical result (Theorem 4) shows that under constant SNR per degree of freedom, the interval-of-overlap goes to one almost surely as the block size N approaches infinity.
- *Simulation performance*: We conduct a number of simulations and show that the computationally efficient binary search method performs similarly to the exhaustive search. In addition, the binary search is asymptotically consistent as the interval length grows.
- *Comparison with neural network approaches*: Given the success of neural networks in image segmentation, considerable work has focused on their application in spectral detection [12]–[17]. We show that the binary search method outperforms custom-trained U-Net neural networks with considerably less complexity.

Related Works

A comprehensive survey of various spectrum sensing methodologies can be found in [1]–[4]. In general, existing approaches can be categorized based on the prior information available regarding the signal and the channel.

The methods proposed in this paper belong to the category of energy detection, first formalized in [18], and later refined in [19]–[22]. These techniques are most applicable when limited or no information about the signal structure is available, relying primarily on the energy variance between signal-plus-noise and noise-only hypotheses. Conversely, when additional information is available, more specialized techniques can be employed [1]. For instance, matched filtering [23], [24] offers optimal detection performance but strictly assumes that the

transmitted signal waveform is known *a priori*, making it unsuitable for non-cooperative or adversarial scenarios. Similarly, feature detection methods [25]–[27] and eigenvalue techniques [28] exploit specific signal properties, such as cyclostationarity or covariance structure, which may not be present or known in arbitrary interfering signals.

In recent years, machine learning and deep learning methods have been widely proposed for the broader problem of signal identification and spectral segmentation. While these data-driven approaches often achieve strong performance, they typically incur high computational complexity [12]–[14]. This presents a significant challenge in real-time and resource-constrained applications—such as spectrum sensing for cognitive radio, adversarial communications, or radar—where large-scale data must be processed with minimal latency. Excessive algorithmic complexity in these scenarios can lead to unacceptable delays, increased energy consumption, or impractical hardware requirements.

Regarding frequency domain processing, many detectors operate on transformed data using fast Fourier transforms (FFTs) [29], filter banks [30], [31], or wavelets [32]–[34]. Our work shares similarities with [29] in its use of frequency-domain data; however, [29] assumes a band structure known *a priori* (e.g., specific WiFi channels). In contrast, our method explicitly addresses the more general and challenging case where the signal may occupy an arbitrary and unknown interval in the frequency domain. Similarly, [35]–[37] presents further examples of deploying transformed data while imposing specific assumptions on signal structure.

Furthermore, edge detection techniques based on the Wavelet Transform (WT) have been explored for wideband sensing [32], [33]. As established in [38], these methods typically treat the Power Spectral Density (PSD) as a train of subbands and utilize Multiresolution Analysis (MRA) to identify singularities (edges) between occupied and vacant bands, often relying on Lipschitz regularity to distinguish signal edges from noise [39]. However, these approaches differ fundamentally from our proposed method in two key aspects: complexity and structural assumptions. First, while robust wavelet sensing often requires the Continuous Wavelet Transform (CWT) or computations across multiple scales M , scaling as $O(M \cdot N \log N)$ [40]–[42], our proposed GLRT-based binary search achieves a linear time complexity of $O(N)$. Second, wavelet methods typically assume the PSD is piecewise smooth to ensure valid edge detection [43], [44], an assumption that may fail under frequency-selective fading or rough signal profiles. Our method avoids these restrictive assumptions, operating robustly on non-coherent power measurements.

It should also be recognized that many transformation-based methods operate under wideband constraints, meaning that the detection data is sampled at a higher rate than the true signal. Several sub-Nyquist strategies have been explored via compressive sensing [45]–[47] and multi-coset sensing [48]. Unlike these approaches, our work does not attempt super-resolution of frequency or time; instead, it focuses on efficient detection within the available degrees of freedom.

Cabric et al. [49], [50] experimentally evaluated spectrum

sensing methods, establishing scaling laws for sensing time in AWGN channels. A key result is that the number of samples required for non-coherent detection methods grows as $1/\text{SNR}^2$ [18], [49], [50], compared to $1/\text{SNR}$ for coherent matched filtering. While we do not derive new scaling laws, our results demonstrate consistent estimation with a constant SNR per bin as the signal length grows.

Finally, while numerous studies have addressed energy efficiency in cognitive radio, the majority focus on minimizing communication-related energy consumption rather than optimizing the computational energy of the detection algorithm itself [51]–[55]. Works that have considered detection complexity have mostly focused on optimizing deep learning architectures [56], [57] or compressive sensing [58]. In this paper, we bridge this gap by proposing a method that is algorithmically efficient by design. In our simulations, we compare it to a custom deep learning method and demonstrate that, even with significantly lower computational complexity, the proposed method offers superior detection performance.

II. PROBLEM FORMULATION

A. Linear Search Problem

For simplicity, we first consider a linear search problem. We are given N frequency bins indexed $n = 0, \dots, N-1$ and a vector of power measurements $\mathbf{X} = (X_0, \dots, X_{N-1})$. A signal occupies an unknown interval $S = [a, b]$ where $0 \leq a \leq b \leq N$ – see Fig. 1(a). Note that a may equal b , so that S is empty. Given the interval S , the received power measurements are modeled as exponential and independent, with an expectation

$$\mathbb{E}[X_n] = \begin{cases} 1 + \gamma & \text{if } n \in S \\ 1 & \text{if } n \notin S, \end{cases} \quad (1)$$

where γ represents an SNR. Here, we have normalized the power values so that $\mathbb{E}(X_n) = 1$ corresponds to the case of a noise only signal.

The assumption of the exponential distribution on the energy per bin is a simplification that can arise as follows: Suppose $X_n = |H_n U_n + W_n|^2$, where H_n is a complex channel gain, U_n is a complex transmitted symbol, and W_n is complex Gaussian noise. Since the receiver is not synchronized with the transmitter, the complex symbol U_n on any particular frequency bin can be modeled as complex Gaussian noise. If we treat the channel gain as deterministic H_n , then X_n will be complex Gaussian with variance $|H_n|^2 \mathbb{E}|U_n|^2 + \mathbb{E}|W_n|^2$. In particular, (1) holds if the noise is normalized to unity, such that $\mathbb{E}|W_n|^2 = 1$ and $\gamma = |H_n|^2 \mathbb{E}|U_n|^2$ are the received energy in bins $n \in S$.

Note that there are two implicit critical assumptions: First, since γ is constant over the entire signal region, we are implicitly assuming that the signal has a constant PSD and that the channel is flat. An interesting avenue for future work is to investigate what happens in cases of frequency-selective fading. Second, by assuming that the noise is normalized to unity, we have assumed that the noise level is known; hence, we assume that the system has undergone a noise estimation process.

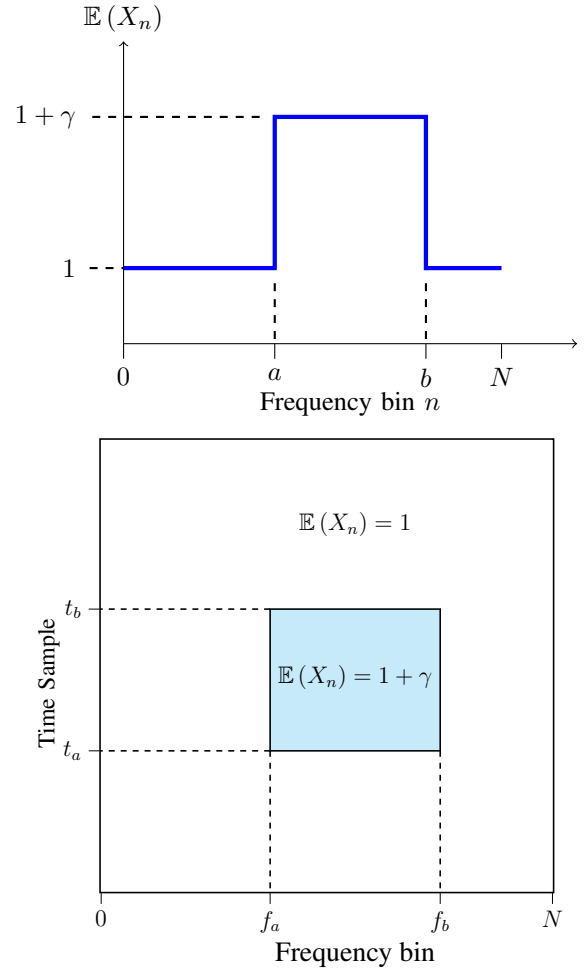


Fig. 1: Detection problem examples: Top: $d = 1$ example for finding an interval $[a, b]$ of signal energy in N frequency bins; Bottom: $d = 2$ example of finding a bounding box in time-frequency.

For exposition, we have considered the single antenna case. The distribution would need to be modified for the multi-antenna case. Specifically, the total noise across N antennas will be a sum of exponential random variables, which follows a chi-squared distribution.

Our problem is twofold: First, we wish to determine whether a signal is present. We model this first problem as a hypothesis testing problem. We denote the null hypothesis by the event $H = 0$, which corresponds to the case when there is no signal. That is, for all n , X_n are i.i.d. exponentially distributed

$$\mathbb{E}[X_n] = 1 \quad \text{for all } n. \quad (2)$$

The case of the null hypothesis ($H = 0$) is identical to (1) in cases where the SNR is $\gamma = 0$. We will denote by $H = 1$ the event that there is a signal in some signal region S with a SNR γ .

Second, if a signal is detected (that is, it is estimated that $H = 1$), we wish to estimate the SNR γ and the signal interval S .

B. Multi-Dimension Extension

The problem is naturally extended to dimensions $d \geq 1$. In this case, \mathbf{X} is a tensor of d -th order with components X_{n_1, \dots, n_d} with $n_i \in [0, N_i]$. For example, \mathbf{X} could be measurements over N_0 time bins and N_1 frequency bins, as you may obtain from N_0 FFTs, each FFT of length N_1 . In the multi-dimensional case, the set S is a hyper-cube:

$$S = \{(n_1, \dots, n_d) \mid a_i \leq n_i < b_i \ \forall i = 1, \dots, d\}, \quad (3)$$

for some left and right intervals $\mathbf{a} = (a_1, \dots, a_d)$ and $\mathbf{b} = (b_1, \dots, b_d)$. As an example, Fig. 1(b) shows a $d = 2$ case for a time-frequency search. The signal region corresponds to a bounding box in time and frequency. Again, we assume that, given S , X_{n_1, \dots, n_d} are exponential and independent with:

$$\mathbb{E}[X_{n_1, \dots, n_d}] = \begin{cases} 1 + \gamma & \text{if } (n_1, \dots, n_d) \in S \\ 1 & \text{if } (n_1, \dots, n_d) \notin S, \end{cases} \quad (4)$$

where, again, γ represents an SNR. To use a uniform notation between the vector and tensor cases, we will let $n = (n_1, \dots, n_d)$ be a d -dimensional tensor index and write the components of the tensor as $X_n = X_{n_1, \dots, n_d}$.

Again, the problem in the multi-dimensional case is to detect whether a signal is present, and if so, to estimate the signal region S and SNR $\gamma > 0$.

III. LIKELIHOOD RATIO TEST

A. Likelihood Function

We follow a standard likelihood ratio detector for the signal detection problem. Let $H = 0, 1$ denote the true signal hypothesis:

$$H = \begin{cases} 0 & \text{no signal present;} \\ 1 & \text{signal is present.} \end{cases} \quad (5)$$

We compute an estimate $\hat{H} = 0, 1$ of H as follows: Let $p(\mathbf{X}|S, \gamma)$ denote the probability density function (PDF) of the measurements of \mathbf{X} for a given signal region S and SNR γ . Also, let $p_0(\mathbf{X}) := p(\mathbf{X}|\emptyset, 0)$ denote the conditional PDF for the null hypothesis $H = 0$ when the signal is not present (i.e., no SNR). Let $J(S, \gamma)$ denote the log likelihood ratio

$$J(S, \gamma) := \log \left[\frac{p(\mathbf{X}|S, \gamma)}{p_0(\mathbf{X})} \right]. \quad (6)$$

Since the parameters γ and S are not known, we use a modified version of the GLRT [10], [11]: We compute the maxima:

$$J_\ell^* := \underset{\substack{S, \gamma \geq 0 \\ |S| = \ell}}{\operatorname{argmax}} J(S, \gamma) \quad (7)$$

where $|S|$ is the cardinality (number of elements) of S . Hence, J_ℓ^* is the maximum over all $\gamma > 0$ and sets S with $|S| = \ell$. We then assume a detector of the form:

$$\hat{H} = \begin{cases} 1 & J_\ell^* \geq t_\ell \text{ for some } \ell \\ 0 & J_\ell^* < t_\ell \text{ for all } \ell, \end{cases} \quad (8)$$

where t_ℓ are a set of thresholds that depend on the set size S . In the standard GLRT, the threshold levels t_ℓ are equal.

However, as we will see below, having a set size-dependent threshold will enable a simpler analysis for the false alarm probability.

For each ℓ , we can compute J_ℓ^* in (7), in two steps: First, for each S , we maximize the likelihood ratio $J(S, \gamma)$ over γ :

$$J(S) := \max_{\gamma \geq 0} J(S, \gamma). \quad (9)$$

Then, J_ℓ^* can be computed by maximizing over S :

$$J_\ell^* = \max_{|S| = \ell} J(S). \quad (10)$$

Our first lemma provides a simple expression for the likelihood ratio and maximization over γ :

Lemma 1. *The likelihood is given by:*

$$J(S, \gamma) = |S| \left[\bar{X}_S \left[\frac{\gamma}{1 + \gamma} \right] - \log(1 + \gamma) \right]. \quad (11)$$

where \bar{X}_S is the average value of X_n on the set S :

$$\bar{X}_S = \frac{1}{|S|} \sum_{n \in S} X_n, \quad (12)$$

The likelihood maximized over the SNR is given by:

$$J(S) = |S| \left[\bar{X}_S^+ - 1 - \log(\bar{X}_S^+) \right]. \quad (13)$$

where

$$\bar{X}_S^+ = \max\{\bar{X}_S, 1\}. \quad (14)$$

Proof. See Appendix A. \square

Using this lemma, we can rewrite the GLRT as follows: Let $\varphi(x)$ be the function:

$$\varphi(x) = x - 1 - \log(x), \quad x \geq 1. \quad (15)$$

Lemma 1 shows that the GLRT (8) can be written as $\hat{H} = 1$ when

$$\ell \varphi(\bar{X}_S^+) \geq t_\ell \text{ for some } |S| = \ell. \quad (16)$$

Since $\varphi(x)$ is increasing for $x \geq 1$, we can define

$$u_\ell = \varphi^{-1}(t_\ell/\ell), \quad (17)$$

and the GLRT estimator (8) is equivalent to:

$$\hat{H} = \begin{cases} 1 & X_S^+ \geq u_{|S|} \text{ for some } S \\ 0 & X_S^+ < u_{|S|} \text{ for all } S. \end{cases} \quad (18)$$

B. False Alarm Probability

Our next result bounds the false alarm probability

$$P_{\text{FA}} = \mathbb{P}(\hat{H} = 1 | H = 0) \quad (19)$$

as a function of the threshold levels u_ℓ in the GLRT (18). This bound will allow us to select the threshold levels. To state the bound, consider the modified GLRT detector (8) (or, equivalently, the GLRT detector in (18)) over a set of hyper-cube regions in (3). Define

$$N = N_1 N_2 \cdots N_d. \quad (20)$$

Each candidate signal region S is defined by a hyper-cube (3) with boundaries \mathbf{a} and \mathbf{b} . Since there are N in (20) choices

for \mathbf{a} and \mathbf{b} , and $\mathbf{b}_i \geq \mathbf{a}_i$, so there are at most $\frac{N^2}{2}$ possible set hyper-cube S . We can then apply a union bound over this set of hypotheses to bound the false alarm probability.

Lemma 2. Consider the modified GLRT detector (18) over a set of hyper-cube regions in (3). Assume that all thresholds satisfy $u_i \geq 0$. Then, the probability of false alarm (19) is bounded above by

$$P_{FA} \leq \frac{N^2}{2} \max_{\ell=1, \dots, N} F(2\ell u_\ell; 2\ell), \quad (21)$$

where N is defined in (20) and $F(s, \nu)$ is the complementary cumulative distribution function (CDF) for a chi-squared random variable with ν degrees of freedom. That is,

$$F(s; \nu) = \mathbb{P}(Z_\nu \geq s), \quad (22)$$

where Z_ν is a chi-squared random variable with ν degrees of freedom.

Proof. See Appendix B. \square

The lemma 2 provides a simple recipe for computing the threshold levels u_ℓ for the GLRT detector in (18), or equivalently, the threshold levels t_ℓ for the GLRT detector in (8). First, we set a desired false alarm probability target P_{FA} . Then, each u_ℓ should satisfy

$$\frac{2P_{FA}}{N^2} = F(2\ell u_\ell; 2\ell). \quad (23)$$

We solve (23) by first computing the value u_ℓ with the inverse complementary CDF:

$$u_\ell = \frac{1}{2\ell} F^{-1} \left(\frac{2P_{FA}}{N^2}; 2\ell \right), \quad (24)$$

Then, we compute t_ℓ from (17)

$$t_\ell = \ell \varphi(u_\ell). \quad (25)$$

Fig. 2 illustrates the threshold values computed using equation 24 for varying signal interval sizes. For smaller intervals, the threshold on the mean power is higher, which is expected since the mean noise power exhibits greater variance over shorter intervals.

C. Probability of Missed Detection

The probability of missed detection is

$$P_{MD} = \mathbb{P}(\hat{H} = 0 | H = 1), \quad (26)$$

which is generally a function of the true signal region S and SNR γ . The following lemma provides a bound on the missed detection probability.

Lemma 3. If the true signal region is S and true SNR is γ , the probability of missed detection is bounded by:

$$P_{MD} \leq 1 - F \left(\frac{2\ell u_\ell}{1 + \gamma}; 2\ell \right), \quad (27)$$

where $\ell = |S|$, where, as before $F(x; \nu)$ is the complementary CDF (22) of a chi-squared random variable with ν degrees of freedom.

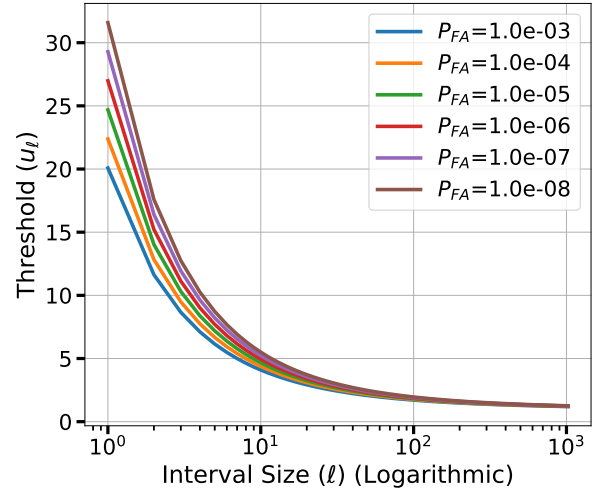


Fig. 2: Threshold values u_ℓ from equation 24 as a function of signal interval size, showing higher thresholds for shorter intervals due to increased noise power variance.

Proof. See Appendix C. \square

It is important to note that changes in noise variance correspond to a scaling of the SNR parameter γ , which is explicitly incorporated in the detection probability analysis (Lemma 3, equation 27). In practice, an increase in noise variance reduces the effective SNR, which, in turn, shifts the detection and missed detection probabilities. However, the false alarm probability remains fixed at the pre-specified level since the thresholds are chosen under the null distribution independently of the signal.

D. Comparison to Known Interval Search

The primary challenge addressed in this paper is the uncertainty associated with the signal interval, denoted as S . To understand the implications of this uncertainty, we can compare the GLRT detector with an equivalent detector that has prior knowledge of the signal interval S . Specifically, consider a scenario in which an oracle provides a singular true potential signal set, denoted as S_0 . In this context, we consider two hypotheses: the null hypothesis H_0 , where the signal is absent, and the alternative hypothesis H_1 , which suggests the presence of a signal within the signal set S_0 . Define $\ell_0 = |S_0|$ as the size of the known signal set, and let u_0 represent the associated threshold value as specified in equation 18. The resulting GLRT detector will simply be:

$$\hat{H} = \begin{cases} 1 & X_{S_0}^+ \geq u_0 \\ 0 & X_{S_0}^+ < u_0. \end{cases} \quad (28)$$

The variable u_0 denotes the threshold level associated with S_0 . According to Section III-B, the expression for P_{FA}^0 and u_0 is given by:

$$P_{FA}^0 = F(2\ell_0 u_0; 2\ell_0), \quad (29)$$

$$u_0 = \frac{1}{2\ell_0} F^{-1}(P_{FA}^0; 2\ell_0), \quad (30)$$

Similarly, as delineated in Section III-C, the expression for P_{MD}^0 may be formulated as follows:

$$P_{\text{MD}}^0 = 1 - F\left(\frac{2\ell_0 u_0}{1 + \gamma}; 2\ell_0\right), \quad (31)$$

Consider the selection of u_0 such that the false alarm probability, P_{FA} , is equal to the predefined threshold P_{FA}^0 . It can be anticipated that the imposition of a more stringent constraint on the false alarm probability P_{FA} will consequently enhance performance concerning the missed detection probability P_{MD} . This improvement reflects the trade-off incurred due to the introduction of interval estimation uncertainty in the proposed methodology. The experimental results concerning this section are elaborated in section VII-B

E. Behavior in Multi-Signal Environments

While the system model in Section II explicitly assumes a single continuous signal interval S , it is valuable to characterize the GLRT detector's behavior in environments containing multiple disjoint signals. In such scenarios, the algorithm seeks the single interval S that maximizes the metric defined in Eq.13. Consequently, the detection outcome depends on the separation distance between the signals. In cases where signals are widely separated by a significant span of noise, the algorithm exhibits a winner-takes-all behavior. Merging two distant signals into a single estimate would require including the intervening noise-only observations, which significantly lowers the average power \bar{X}_S . Since the term $[\bar{X}_S - 1 - \log(\bar{X}_S)]$ in the likelihood function diminishes rapidly as \bar{X}_S approaches the noise floor of 1, the penalty for including a large noise gap typically outweighs the linear gain in degrees of freedom $|S|$. As a result, the detector converges on the single signal component that yields the highest individual likelihood score. Conversely, if the signals are closely spaced, the algorithm is likely to merge them into a single aggregate interval, as the likelihood gain from capturing the energy of the second signal outweighs the penalty introduced by the short noise segment between them.

IV. COMPUTATIONALLY EFFICIENT BINARY SEARCH

A. Dyadic Interval Detection

The GLRT detector in (8) requires searching over all possible signal regions S . We will call this method *exhaustive maximum-likelihood (ML)*. As discussed above, there are $\approx N^2/2$ such signal regions where N is given by the product (20). Hence, the complexity of exhaustive ML will be $O(N^2)$, which may be challenging, particularly at high sample rates.

In this section, we propose a simplified search method for the linear search case where $d = 1$. Exhaustive ML in this case has a complexity $O(N^2)$. The proposed method will have a complexity $O(N)$.

The key to the algorithm is to perform a binary search on a set of *dyadic intervals*. We assume $N = 2^M$ for some $M \geq 0$. The dyadic intervals are

$$I_{m,i} = [i2^m, (i+1)2^m) \subseteq [0, 1, \dots, N), \quad (32)$$

where $m = 0, \dots, M$ and $i = 0, \dots, 2^{M-m} - 1$. We will call $I_{m,i}$ the i -th dyadic interval at the m -th level. The proposed algorithm, which we call *binary search*, operates in two phases:

- *Initial interval detection* where we search the set of dyadic intervals to detect whether a signal is present.
- *Binary interval estimation*: If a signal is detected in the dyadic interval search, the most likely interval is estimated using a binary search.

Algorithm 1 Initial Interval Search

Require: Interval length $N = 2^M$

Require: Power measurements $X_n, n = 0, \dots, N - 1$

Require: Threshold levels $u_k, k = 1, 2, 4, \dots, 2^M$

```

1:  $\hat{H} \leftarrow 0$ 
2: for  $m = 0, \dots, M$  do
3:    $\ell \leftarrow 2^m$  // interval length
4:    $k \leftarrow 2^{M-m}$  // number of intervals
5:    $Z_m^* \leftarrow 0$ .
6:   for  $i = 0, \dots, k - 1$  do
7:     if  $m = 0$  then
8:        $Z_{0,i} \leftarrow X_i$ 
9:     else
10:       $Z_{m,i} \leftarrow (Z_{m-1,2i} + Z_{m-1,2i+1})/2$ .
11:    end if
12:    if  $Z_{m,i} \geq u_k$  then
13:       $Z_m^* \leftarrow Z_{m,i}$ 
14:       $i_m^* \leftarrow i$ 
15:    end if
16:  end for
17:  if  $Z_m^* \geq u_k$  then
18:     $\hat{H} \leftarrow 1$ 
19:     $J_m^* \leftarrow \ell(Z_m^* - 1 - \log(Z_m^*))$ 
20:  end if
21: end for
22: if  $\hat{H} = 1$  then
23:    $\hat{m} \leftarrow \operatorname{argmax}_m J_m^*$ 
24:    $\hat{i} \leftarrow i_m^*$ 
25:   return  $(\hat{H} = 1, \hat{m}, \hat{i})$ 
26: else
27:   return  $\hat{H} = 0$ 
28: end if

```

In this subsection, we describe the first stage, namely the dyadic interval search. The precise steps are shown in Algorithm 1. In this algorithm, we start with N intervals, each representing a power measurement bin X_i . At each stage, we sequentially merge adjacent intervals and compute X_S for all resulting intervals. It can be verified that:

$$Z_{m,i} = \bar{X}_S \text{ for } S = I_{m,i}, \quad (33)$$

So, the algorithm computes the mean energy over all the dyadic intervals. The resulting estimate is then:

$$\hat{H} = \begin{cases} 1 & \text{if } \bar{X}_S \geq u_{|S|} \text{ for some } S = I_{m,i} \\ 0 & \text{if } \bar{X}_S < u_{|S|} \text{ for all } S = I_{m,i}. \end{cases} \quad (34)$$

Hence, Algorithm. 1 produces a hypothesis estimate \hat{H} that

matches the estimate for the GLRT detector (18), except that the search is only over the dyadic intervals $S = I_{m,i}$ as opposed to all subsets.

B. Interval Estimation

If a signal has been detected by Algorithm 1, we then obtain an estimate for the interval by Algorithm 2. This algorithm takes as inputs the binary energy values $Z_{m,i}$ from Algorithm. 1. If the signal length is $N = 2^M$, the algorithm proceeds in M iterations indexed by $t = 0, \dots, M - 1$. In each iteration, it finds an estimate for the interval of the form:

$$\widehat{S}^{(t)} = [\widehat{a}^{(t)}, \widehat{b}^{(t)}], \quad (35)$$

where the left and right boundaries $\widehat{a}^{(t)}$ and $\widehat{b}^{(t)}$ are of the form:

$$\widehat{a}^{(t)} = \widehat{i}^{(t)} \ell_t, \quad \widehat{b}^{(t)} = \widehat{j}^{(t)} \ell_t, \quad \ell_t = 2^{M-t}, \quad (36)$$

so that they are restricted to discrete values:

$$\widehat{a}^{(t)}, \widehat{b}^{(t)} \in \{0, \ell_t, 2\ell_t, \dots, N\}.$$

We call the spacing ℓ_t the *sub-interval length* in iteration t . Hence, the algorithm finds iteratively finer estimates of the interval boundaries since the sub-interval length ℓ_t decreases as t increases. Initially, the algorithm takes the estimates

$$\widehat{S}^{(0)} = [\widehat{a}^{(0)}, \widehat{b}^{(0)}] = [0, N], \quad (37)$$

corresponding to the entire interval.

At each iteration, it then iteratively refines first the estimate for the left boundary $\widehat{a}^{(t)}$ and then the right boundary $\widehat{b}^{(t)}$. The update for the left boundary searches over candidates:

$$\widehat{a}^{(t+1)} \in \{\widehat{a}^{(t)} - \ell_{t+1}, \widehat{a}^{(t)}, \widehat{a}^{(t)} + \ell_{t+1}\} \quad (38)$$

so that it searches over one index to the right and left. For each candidate, $\widehat{a}^{(t+1)}$, the algorithm evaluates the objective $J([\widehat{a}^{(t+1)}, \widehat{b}^{(t)}])$ where $J(S)$ is the likelihood in (13). Similarly, the optimization over the right boundary searches over values for $\widehat{b}^{(t+1)}$ in the set:

$$\widehat{b}^{(t+1)} \in \{\widehat{b}^{(t)} - \ell_{t+1}, \widehat{b}^{(t)}, \widehat{b}^{(t)} + \ell_{t+1}\}, \quad (39)$$

so that it searches over one index to the left and right.

C. Complexity

The algorithm 1 comprises $\log_2(N)$ steps, within each of which the energy is assessed across $N/2^m$ intervals. Consequently, $O(N)$ computations are required in total to determine the energy of all intervals. For Algorithm 2, there are two key computational savings. First, each evaluation of $J(S)$ does not require recomputing the average energy \bar{X}_S . Recomputing \bar{X}_S directly requires taking a sum over $|S|$ elements, which can be as large as N . However, the algorithm uses the pre-computed values $Z_{m,i}$ to compute \bar{X}_S . Secondly, the search involves only $M = \log_2(N)$ iterations, and in each iteration, there is a bounded number of operations. Hence, the overall complexity of Algorithm 2 is $O(\log_2(N))$. So, the proposed method, which is the union of the two algorithms, has an overall complexity of $O(N)$.

Algorithm 2 Binary Interval Estimation

Require: Interval length $N = 2^M$

Require: Dyadic powers $Z_{m,i}$

```

1:  $\widehat{i}^{(0)} \leftarrow 0$  // initial left index
2:  $\widehat{j}^{(0)} \leftarrow 1$  // initial right index
3:  $\widehat{Z}^{(0)} = Z_{M,0}$ , // initial average energy
4:  $\widehat{L}^{(0)} \leftarrow N = 2^M$  // initial interval length
5:  $\ell_0 \leftarrow 2^M$  // initial sub-interval length
6:  $Z^+ = \max\{\widehat{Z}^{(0)}, 1\}$ 
7:  $J_{\max} = \widehat{L}^{(0)}[Z^+ - 1 - \ln(Z^+)]$  // initial objective
8:
9: for  $t = 0, \dots, M - 1$  do
10: // Get layer info
11:  $m \leftarrow M - t - 1$  // layer
12:  $\ell_{t+1} \leftarrow 2^m$  // sub-interval length
13:
14: // Optimization over left boundary
15:  $\widetilde{Z}^{(t)} \leftarrow \widehat{Z}^{(t)}$ ,  $\widehat{i}^{(t+1)} \leftarrow 2\widehat{i}^{(t)}$ ,  $\widetilde{L}^{(t)} \leftarrow \widehat{L}^{(t)}$ 
16: for  $\delta \in \{-1, 1\}$  do
17:  $i' \leftarrow 2\widehat{i}^{(t)} + \delta$ 
18:  $L' \leftarrow \widetilde{L}^{(t)} - \delta\ell_{t+1}$ 
19:  $Z' \leftarrow (\widetilde{L}^{(t)}\widetilde{Z}^{(t)} - \delta\ell_{t+1}Z_{m,i'})/L'$ 
20:  $J' \leftarrow L'[(Z^+ - 1) - \ln(Z^+)]$ ,  $Z^+ = \max\{Z', 1\}$ 
21: if  $J' > J_{\max}$ ,  $L' \geq 0$ , and  $i' \geq 0$  then
22:  $J_{\max} \leftarrow J'$ 
23:  $\widehat{i}^{(t+1)} \leftarrow i'$ 
24:  $\widetilde{Z}^{(t)} \leftarrow Z'$ ,  $\widetilde{L}^{(t)} \leftarrow L'$ 
25: end if
26: end for
27:
28: // Optimization over right boundary
29:  $\widetilde{Z}^{(t+1)} \leftarrow \widetilde{Z}^{(t)}$ ,  $\widehat{j}^{(t+1)} \leftarrow 2\widehat{j}^{(t)}$ ,  $\widetilde{L}^{(t+1)} \leftarrow \widetilde{L}^{(t)}$ 
30: for  $\delta \in \{-1, 1\}$  do
31:  $j' \leftarrow 2\widehat{j}^{(t)} + \delta$ 
32:  $L' \leftarrow \widetilde{L}^{(t)} + \delta\ell_{t+1}$ 
33:  $Z' \leftarrow (\widetilde{L}^{(t)}\widetilde{Z}^{(t)} + \delta\ell_{t+1}Z_{m,j'})/L'$ 
34:  $J' \leftarrow L'[(Z^+ - 1) - \ln(Z^+)]$ ,  $Z^+ = \max\{Z', 1\}$ 
35: if  $J' > J_{\max}$ ,  $L' > 0$ , and  $j' \leq 2^{t+1}$  then
36:  $J_{\max} \leftarrow J'$ 
37:  $j^{(t+1)} \leftarrow j'$ 
38:  $\widetilde{Z}^{(t+1)} \leftarrow Z'$ ,  $\widetilde{L}^{(t+1)} \leftarrow L'$ 
39: end if
40: end for
41: end for

```

V. ASYMPTOTIC CONSISTENCY OF THE BINARY SEARCH

In this section, we prove that the binary interval estimation algorithm, Algorithm 2, is asymptotically consistent in the limit of large N under a fixed SNR per bin γ . Specifically, we consider the $d = 1$ dimensional case and examine a sequence of problems indexed by the total length N . We fix a “true” SNR γ and assume that the true signal interval

$$S_N^0 = [a_N^0, b_N^0], \quad a_N^0 = \lfloor \alpha_0 N \rfloor, \quad b_N^0 = \lfloor \beta_0 N \rfloor, \quad (40)$$

for some constants $0 < \alpha_0 < \beta_0 < 1$ that do not depend on N . Assume that X_n , $n = 0, \dots, N$ are generated i.i.d. from

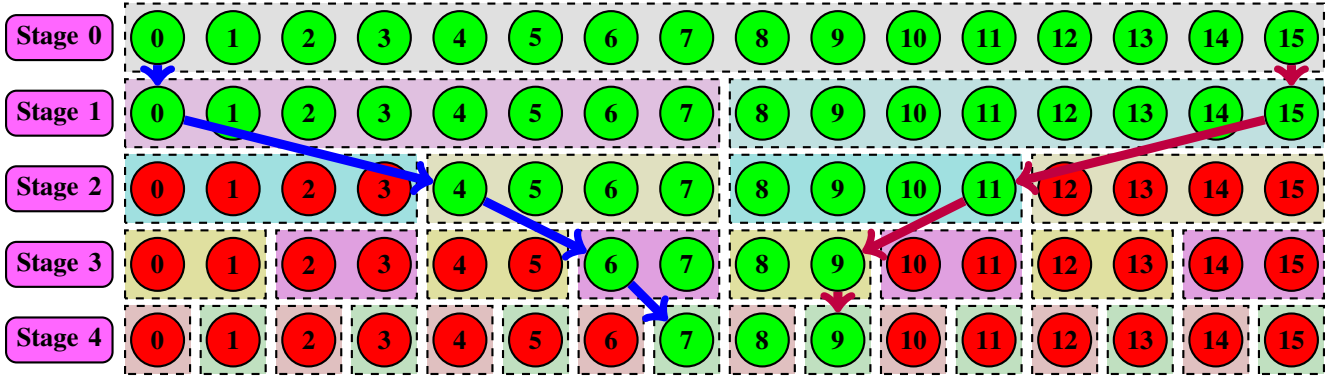


Fig. 3: The diagram illustrates the computationally efficient maximum likelihood method using binary search over possible intervals. The figure demonstrates the method for $N = 16$, where N represents the number of power measurements. The blue and purple lines respectively depict the trajectory of the detected start and end of the optimal interval across different stages. The signal, detected within the interval $X_{[7,9]}$, is highlighted by green circles.

the model (1). We let $\hat{a}_N^{(t)}, \hat{b}_N^{(t)}$ be the outputs of Algorithm 2, and let $\hat{S}_N^{(t)}$ denote the corresponding interval:

$$\hat{S}_N^{(t)} = [\hat{a}_N^{(t)}, \hat{b}_N^{(t)}) \quad (41)$$

A common metric for the performance of the algorithm is the so-called intersection over union, or IoU:

$$\text{IoU}_N^{(t)} = \frac{|\hat{S}_N^{(t)} \cap S_N^0|}{|\hat{S}_N^{(t)} \cup S_N^0|}. \quad (42)$$

Although the true interval is modeled as deterministic, the estimated interval $\hat{S}_N^{(t)}$ and, hence, the performance metric $\text{IoU}_N^{(t)}$ are random.

Theorem 4. *Under the above assumptions*

$$\lim_{N, t \rightarrow \infty} \text{IoU}_N^{(t)} = 1 \quad (43)$$

almost surely.

Proof. See Appendix D \square

This asymptotic consistency result (Theorem 4) is important because it establishes that the proposed binary interval estimation algorithm reliably identifies the correct signal interval in the limit of large measurement sizes. Practically, this means that as more data is collected (larger N) and the algorithm is allowed sufficient refinement steps (larger t), the estimated interval converges exactly to the signal region identified by the exhaustive algorithm, guaranteeing high accuracy in signal detection tasks.

VI. BASELINE NEURAL NETWORKS

It is important to compare the proposed algorithm to widely-used U-Net networks. The U-Net architecture is widely used in segmentation and detection tasks [59]–[61], and has also been proposed for spectral segmentation and signal detection [62]–[66]. Our simulations below will show that the proposed method offers both improved complexity and performance compared to U-Nets.

We selected the Convolutional Neural Network (CNN)-based U-Net architecture as our primary baseline because

it remains the de facto standard for semantic segmentation in signal processing, effectively capturing the local coherence required to detect contiguous signal intervals. While newer architectures, such as Transformers or hybrid CNNs-Transformers, excel in tasks requiring long-range dependency modeling, they typically incur significantly higher computational costs—often scaling quadratically ($O(N^2)$) due to self-attention mechanisms—compared to the efficiency of CNNs. Given that the proposed binary search method already operates near the theoretical detection bound with linear $O(N)$ complexity, employing a heavier Transformer baseline would primarily widen the computational gap without yielding statistically significant performance gains over the theoretical limit. Thus, the U-Net serves as a robust and sufficient benchmark to illustrate the trade-off between deep learning complexity and our efficient algorithmic approach.

For the one-dimensional case, we consider the U-Net depicted in Fig. 4. For higher-dimensional data, the standard U-Net architecture is employed, with a sufficient number of encoding and decoding stages and appropriately scaled data and filter sizes. In each stage, a two-step convolutional block is applied. This block consists of a convolution operation, followed by Batch Normalization and ReLU activation, and is concluded with a Max-Pooling layer to downsample the signal by a factor of two. During the encoding stages, feature map information is progressively captured across multiple channels, culminating in M channels of 1×1 data. This process parallels the proposed binary search method. Initially, $J(S)$ is computed over the entire interval, similar to the first stage of the U-Net encoder. The search is then refined over progressively smaller intervals, analogous to the subsequent encoder stages of the U-Net, until the signal is examined in each bin corresponding to the final stage of the U-Net encoder.

In the decoding phase, similar to the conventional U-Net architecture, we iteratively up-sample the feature maps and concatenate them with the corresponding encoder feature maps. A similar convolutional block is then applied to the concatenated feature maps. This process continues until we obtain a two-channel output segmentation map, where a $\text{Conv}1 \times 1$ layer is used to generate the final segmentation mask. Intuitively, the

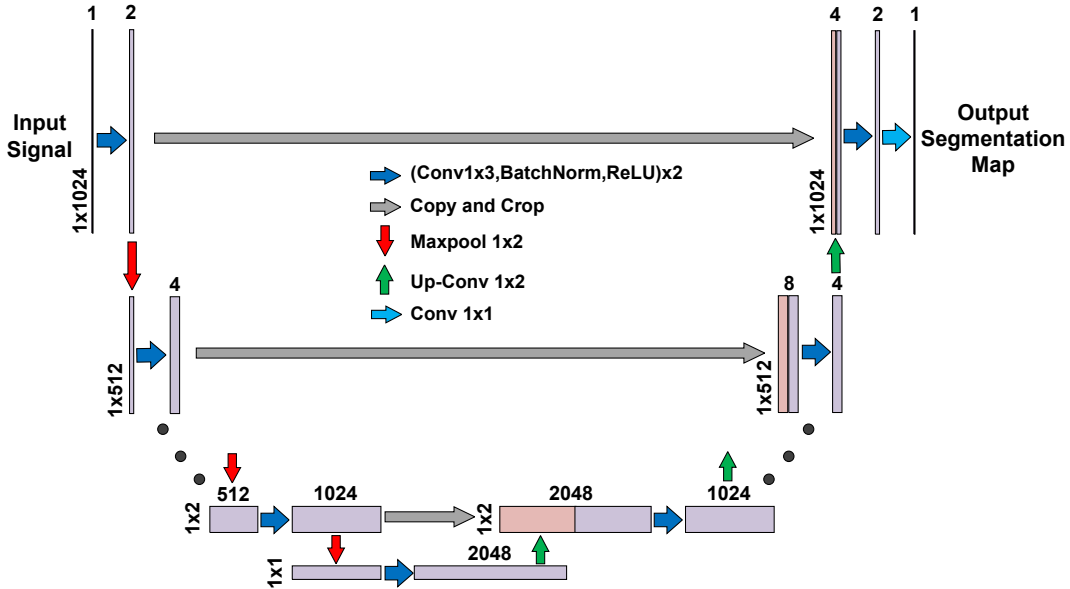


Fig. 4: The architecture of the baseline U-Net used for signal detection in this paper. This architecture is designed for one-dimensional data. However, the same principles and methods can be extended to handle higher-dimensional data. For each feature map, dimensions are annotated at the bottom left, while the number of channels is indicated at the top. As illustrated in the figure, the process initiates with the input signal, upon which a convolutional block comprising two stages of 1×3 convolution, Batch Normalization, and ReLU activation is applied. This is followed by a Max Pooling operation, which is iteratively repeated until achieving a 1×1 feature map with 2048 channels. The decoding phase commences with up-convolutions, wherein feature maps are concatenated with the corresponding encoder maps, applying the same convolutional block utilized during the encoding stage. Finally, a Conv 1×1 layer is employed to generate the output segmentation map.

decoder seeks to reconstruct the signal interval information from the encoded channels using convolutional blocks, which parallels the functionality of our binary search algorithm.

VII. EXPERIMENTAL RESULTS

Our goal is to compare the detection accuracy and signal set estimation error of the proposed binary search method to more complex exhaustive ML. Additionally, for the signals that are detected, we will compare the estimation error to a trained U-Net. We consider two scenarios for these comparisons:

- *1D detection*: We take $N = 1024$ points. When a signal is present, it is in an unknown interval with variable length ℓ and variable SNR.
- *2D detection*: We take $N = 128 \times 128$ points. When a signal is present, it is on an unknown square of size $\ell \times \ell$ and variable SNR.

Specifically, the received power measurements X_n are modeled as independent exponential random variables with a mean $\mathbb{E}[X_n] = 1 + \gamma$ if the bin n belongs to the signal region S , and $\mathbb{E}[X_n] = 1$ otherwise. This corresponds to a standard non-coherent energy detection setup, where γ represents the SNR. We train U-Nets for each of the two cases. In both cases, we generate a dataset of $n = 200,000$ samples. Since the U-Net is only used for the estimation of the signal set, all n samples have a signal present. Hence, each sample i can be represented as a pair (X_i, S_i) , where X_i is the vector or array of power values, and S_i is the true signal interval. We vary the SNR in

TABLE I: Summary of hyperparameters and settings used for U-Net training and evaluation.

Hyperparameter	Value
Optimization Algorithm	Adam
Initial Learning Rate	10^{-2}
Learning Rate Scheduler	StepLR
Batch Size	64
Number of Training Epochs	50
Training Loss Function	Binary Cross-Entropy (BCE)
Evaluation Metric	Intersection over Union (IoU)
U-Net Parameters (1D)	43,380,007
U-Net Parameters (2D)	1,949,011
PyTorch Version	2.6.0

the samples from -3 dB to 20 dB, with an emphasis on lower SNRs. For the 1D case, the interval size is varied from 1 to 256, and in the 2D case ℓ is varied from 1 to 64. The dataset is divided into training and test sets with an 80/20% ratio. A summary of the hyperparameters and settings used for the training and evaluation of the U-Net is provided in Table I.

For detection accuracy, we fix the threshold for a false alarm rate of 10^{-6} using the bound in Lemma 2. For every candidate interval, the corresponding threshold t_ℓ is calculated and subsequently employed within the GLRT detector. In our experiments, we adopt a stringent false alarm probability of $P_{FA} = 10^{-6}$ to reflect the requirements of practical spectrum sensing and adversarial detection scenarios, where false alarms can incur significant operational costs. This

TABLE II: Comparison of number of floating point operations (FLOPs) needed for the proposed binary search method, exhaustive ML method, and U-Net

Algorithm	Number of FLOPs	
	1D-1024	2D-128×128
Exhaustive ML	5.24×10^6	7.27×10^8
U-Net	4.0×10^7	10^7
Binary Search (Proposed Method)		
Algorithm 1	3.13×10^3	2.86×10^4
Algorithm 2	6.2×10^2	9.1×10^2
Binary Search-Total	3.75×10^3	2.95×10^4

conservative setting intentionally imposes a higher detection threshold, thereby creating a challenging test environment for the proposed method. As will be detailed later, despite this stringent constraint, the proposed binary-search-based detector exhibits consistently high detection performance, demonstrating its robustness and effectiveness under low-SNR and high-uncertainty conditions. Figures. 6 and 8 show the missed detection rates for exhaustive ML and binary search methods. We observe that in the 1D case, the detection is no worse than 3 dB and no worse than 6 dB in the 2D case. This difference is explicable since, in the worst case, the binary search captures 1/2 the energy in the 1D case and 1/4 the energy in the 2D case. Importantly, as the interval sizes increase, the gap decreases, indicating that the proposed method has minimal loss for larger interval sizes.

Figures. 5 and 7 show the estimation accuracy for the detected signals. Here, we compare the exhaustive ML, binary search, and U-Net. For all three, we plot the detection intersection over union (IOU) error rate, defined as:

$$\text{IOU Error Rate} = 1 - \frac{S \cap \hat{S}}{S \cup \hat{S}} \quad (44)$$

where S represents the ground-truth interval and \hat{S} corresponds to the estimated interval. From the figures, we see that for any SNR, as the interval sizes increase, the detection error rate approaches zero, as predicted by Theorem 4. Second, for larger interval sizes, the gap between the exhaustive ML and binary search decreases, again suggesting that the proposed method will perform well for larger intervals.

Finally, the proposed method significantly outperforms U-Net in most interval sizes. This improvement in performance occurs even though the proposed binary search method is significantly simpler. As a way to compare, we can count the number of operations for detection (Algorithm. 1), binary interval estimation (Algorithm. 2), exhaustive ML, and U-Net. Table. II and Fig. 9 present a comprehensive summary of the floating point operations required for each algorithm considered. These figures were estimated using a Python-based simulator (utilizing standard NumPy, SciPy, and PyTorch libraries). As evidenced by the data in the table, the proposed binary search algorithm requires significantly fewer operations—by several orders of magnitude—compared to both U-Net and exhaustive ML methods, applicable to both 1D and 2D scenarios.

A. Effect of Noise Estimation

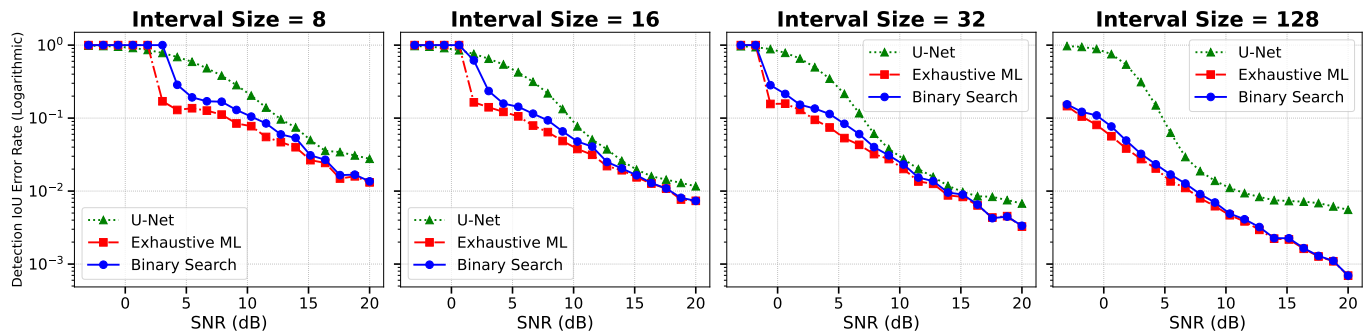
Up to this point, we have implicitly assumed that the noise variance is perfectly known and normalized to unity. In practical systems, however, the noise power must be estimated during a calibration phase, and any estimation error can impact subsequent detection performance. To quantify the effect of imperfect noise estimation, we conduct the following experiment. Let N_{ref} denote the number of degrees of freedom allocated for noise power estimation. During the calibration, it is assumed that no signals are present and that the received samples consist purely of noise. The noise variance is then estimated as $\hat{\sigma}^2 = \frac{1}{N_{\text{ref}}} \sum_{i=1}^{N_{\text{ref}}} |w_i|^2$, where $(w_i \sim \mathcal{CN}(0, \sigma^2))$ are independent noise samples. This estimator follows a scaled chi-squared distribution with $(2N_{\text{ref}})$ degrees of freedom, implying that its relative variance decreases as $(1/N_{\text{ref}})$. Subsequently, in the detection phase, the received samples are normalized using the estimated noise power, i.e., $X'_n = \frac{X_n}{\hat{\sigma}}$, where X_n represents the received samples, and X'_n denotes the normalized samples, respectively. The detection statistic is then computed based on X'_n , assuming unity noise variance, even though the true noise level may differ due to estimation error. We evaluate the resulting detection performance by plotting the detection IOU error rate and the probability of missed detection (P_{MD}) versus SNR for different values of N_{ref} , as illustrated in Fig. 10. This analysis highlights the trade-off between calibration overhead and detection accuracy: a larger (N_{ref}) yields more reliable noise estimates and better detection performance, whereas a smaller (N_{ref}) leads to higher variance in the estimated noise power and degraded performance.

B. Performance Comparison With an Oracle Interval Detector

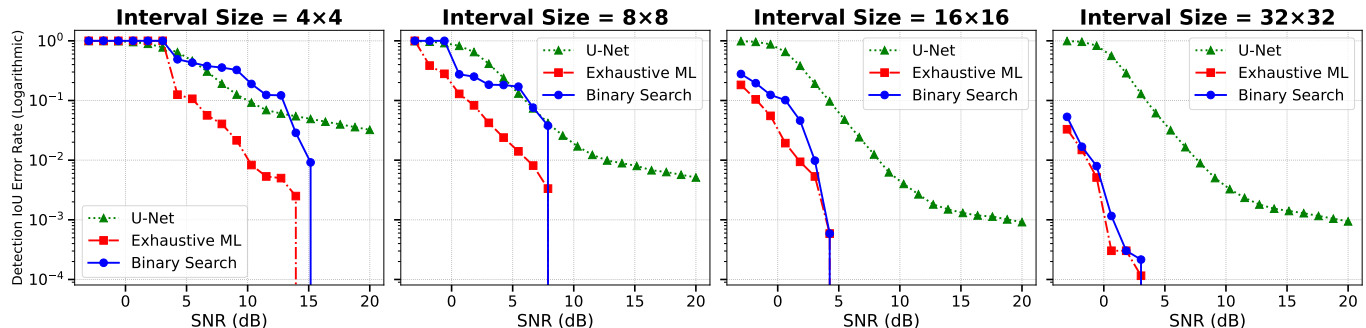
The key challenge addressed in this work is that the signal is unknown and must be estimated jointly with detection. To illustrate the resulting performance impact, we compare the detector performance when the signal interval is not known with that of an oracle detector that has perfect knowledge of the true interval. Accordingly, we repeat the experiments described in Section VII, now including the oracle detector as a benchmark to assess the role of interval knowledge (S), as discussed in Section III-D. The results, shown in Fig. 11, indicate that when the signal interval is known a priori (oracle case), the detector achieves substantially better performance, yielding a lower missed-detection probability (P_{MD}) at a fixed false-alarm rate (P_{FA}^0). In contrast, the proposed GLRT detector—which must infer the signal interval—incurs a moderate performance loss due to this additional uncertainty. This comparison quantitatively highlights the degradation introduced by interval uncertainty and confirms the theoretical trade-off between detection sensitivity and false-alarm control.

C. Performance Analysis

To rigorously evaluate the proposed method, we selected comparison baselines that bound performance from both theoretical and data-driven perspectives. The Exhaustive Maximum Likelihood method serves as the theoretical upper bound for



(a) The detection IOU error rate of different methods for different SNRs (false alarm rate fixed at 10^{-6}) for the one-dimensional data.



(b) The detection IOU error rate of different methods for different SNRs (false alarm rate fixed at 10^{-6}) for the two-dimensional data.

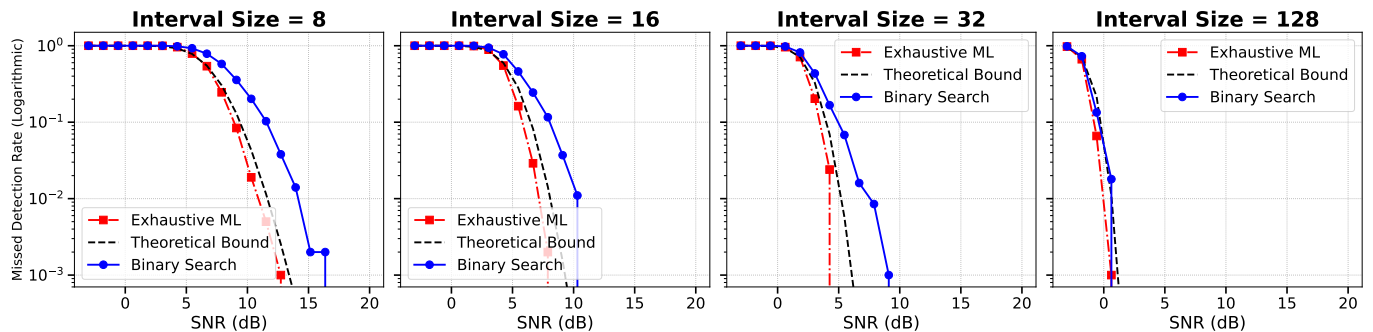
Fig. 5: The detection IOU error rate of the exhaustive and binary search maximum likelihood estimations and U-Net for 1D and 2D signals with SNRs ranging from -3 to 20 dB. Each plot represents the performance for a specific fixed signal size. As expected, increasing the SNR improves the performance of both methods. The figures indicate that the performance of the two methods is nearly identical for larger signal sizes. For smaller signal sizes, the binary search method still performs similarly to the exhaustive ML at low and high SNRs, with only a slight, non-significant performance drop observed at intermediate SNRs. In most cases, the binary search ML method surpasses the U-Net in the IOU metric while maintaining significantly lower computational complexity. The performance is generally better for 2D data compared to 1D data.

detection performance. As derived in Lemma 1, the Exhaustive ML constitutes the optimal detector for the unknown interval problem under the exponential model. By benchmarking against this optimal standard, we quantify the precise performance trade-off incurred by the computational efficiency of our approach. The results in Figures. 6 and 8 demonstrate that the proposed Binary Search algorithm maintains performance within 3 dB of this theoretical limit (in the 1D case), validating its near-optimal efficacy.

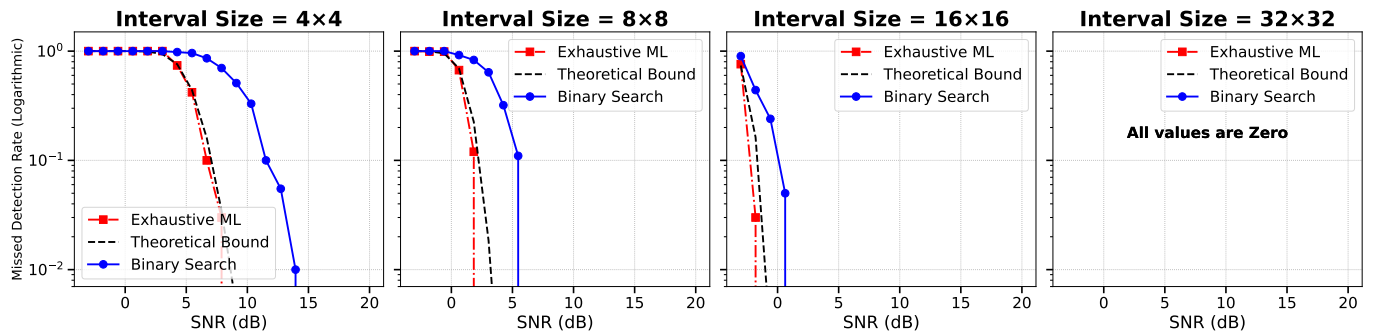
Conversely, the U-Net architecture was selected to represent state-of-the-art, high-complexity Deep Learning (DL) approaches. While DL methods are increasingly popular for spectral segmentation, comparing them against U-Net highlights that our statistically derived GLRT approach achieves superior IOU and detection rates (Figures. 5 and 7) without the massive computational overhead (Table II) or the extensive training data requirements inherent to neural networks. We prioritized these baselines over wavelet-based or edge-detection techniques, as the latter often rely on signal smoothness assumptions that may not hold for the non-coherent power measurements considered here, and typically incur higher computational complexity ($O(M.N \log N)$ where M is the number of analyzed scales) compared to the $O(N)$ efficiency of our proposed method.

The superior performance of the proposed estimator in terms of False Alarm Probability (FAP), and detection probability stems from two fundamental properties of the GLRT:

- Analytically Controlled FAP: Unlike heuristic edge detectors or neural networks, where the FAP is often empirical, our method ensures a strict Constant False Alarm Rate. As established in Lemma 2, we derive a closed-form bound for the false alarm probability based on the Chi-squared distribution. This allows for the precise calculation of thresholds u_l required to meet a specific target P_{FA} (e.g., 10^{-6}). This rigorous statistical control minimizes false positives more effectively than learning-based models, which may be susceptible to hallucinated signals due to distribution shifts in the training data.
- Optimized Signal-to-Noise Integration: Standard energy detectors with fixed bandwidths inevitably suffer from noise integration when the signal bandwidth is unknown, as they integrate noise over empty frequency bins. In contrast, our method dynamically estimates the interval of overlap S . By refining the start and end points of the signal, the detector maximizes the normalized average energy metric derived in Eq. 13. This ensures that the detection statistic is computed primarily over signal-occupied bins, effectively maximizing the SNR



(a) The missed detection rate of maximum likelihood methods for different SNRs (false alarm rate fixed at 10^{-6}) for the one-dimensional data.



(b) The missed detection rate of maximum likelihood methods for different SNRs (false alarm rate fixed at 10^{-6}) for the two-dimensional data.

Fig. 6: The missed detection rate of the exhaustive and binary search maximum likelihood estimations and U-Net for 1D and 2D signals with SNRs ranging from -3 to 20 dB. Each plot represents the performance for a specific fixed signal size. As expected, increasing the SNR improves the performance of both methods.

and resulting in higher detection probabilities compared to methods that cannot precisely localize the interval.

VIII. CONCLUSION

In this paper, we investigate signal detection challenges in environments characterized by unknown signal bandwidth and occupancy intervals, particularly under adversarial and spectrum-sharing conditions. We introduced an effective GLRT-based approach that leverages normalized average signal energy as a straightforward yet powerful detection metric. Our theoretical analysis provided bounds for false alarm and missed detection probabilities, explicitly linking them to the SNR and the size of the signal set. Addressing the significant computational overhead inherent in exhaustive search methods, we proposed a computationally efficient binary search algorithm that reduces the complexity from $O(N^2)$ to $O(N)$ in one-dimensional scenarios. Notably, this binary search method achieves performance comparable to exhaustive searches and demonstrates asymptotic consistency, ensuring that the interval-of-overlap converges to unity under constant SNR conditions as the measurement size grows. Our comprehensive simulation studies validated the efficacy and efficiency of the proposed binary search method. The method not only maintained near-optimal performance relative to exhaustive searches but also demonstrated superior detection capabilities and significantly lower computational complexity

compared to contemporary neural network-based approaches, notably outperforming specialized U-Net models. In conclusion, our proposed GLRT-based binary search approach provides a robust and computationally efficient solution for signal detection in uncertain spectral environments, promising substantial practical benefits for spectrum sensing applications, especially in resource-constrained systems. Future work will include comparisons with benchmark receivers that exploit known structural attributes. Additionally, significant attention will be directed towards addressing the important case of multiple simultaneous signals and the development of more realistic models for signals that are not exactly aligned with the degrees of freedom.

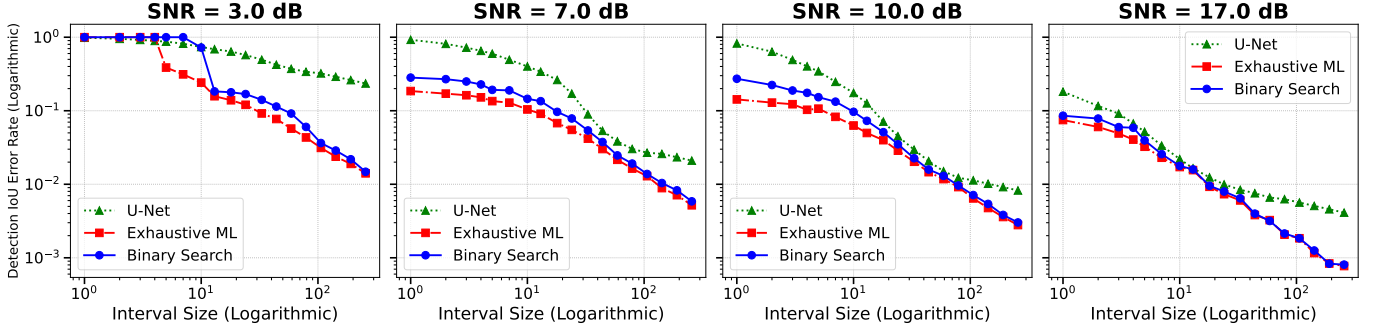
APPENDIX A PROOF OF LEMMA 1

Given any signal region S and SNR γ , each X_n is exponentially distributed as

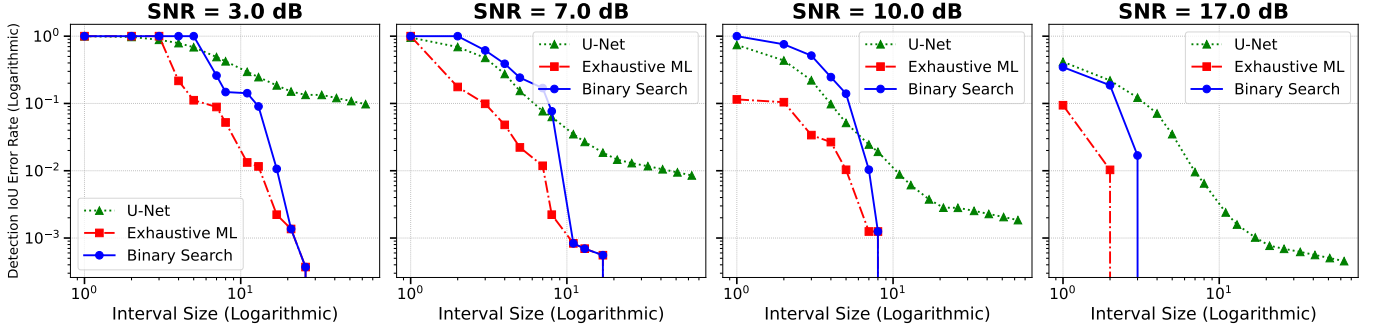
$$p(X_n|S, \gamma) = \lambda_n^{-1} e^{-X_n/\lambda_n}, \quad (45)$$

where

$$\lambda_n = \begin{cases} 1 & \text{if } n \notin S, \\ 1 + \gamma & \text{if } n \in S, \end{cases} \quad (46)$$



(a) The detection IOU error rate of different methods for different signal sizes (false alarm rate fixed at 10^{-6}) for the one-dimensional data.



(b) The detection IOU error rate of different methods for different signal sizes (false alarm rate fixed at 10^{-6}) for the two-dimensional data.

Fig. 7: The detection IOU error rate of the exhaustive and binary search maximum likelihood estimations and U-Net for 1D and 2D signals with sizes ranging from 1 to 256 (out of $N = 1024$) for 1D and 1 to 64 (out of $N = 128$) for 2D. Each plot represents the performance for a specific fixed signal SNR. Increasing the signal size improves the performance of both methods, as detecting smaller signals is more challenging. As shown in the figure, the binary search method exhibits a slight, non-significant performance drop, which is less pronounced for larger SNRs. Similar to Fig. 5, the performance of both methods is much closer for very small and very large signal sizes. Similarly in most cases, the binary search ML method outperforms the U-Net in the IOU metric while keeping lower computational complexity. The performance is generally better for 2D data compared to 1D data.

Therefore,

$$\begin{aligned} \log \frac{p(\mathbf{X}|S, \gamma)}{p_0(\mathbf{X})} &= \log \prod_{n \in S} \left[\frac{1}{1 + \gamma} \exp(X_n(1 - 1/(1 + \gamma))) \right] \\ &= -|S| \log(1 + \gamma) + \left[\frac{\gamma}{1 + \gamma} \right] \sum_n X_n \\ &= |S| \left[\bar{X}_S \left[\frac{\gamma}{1 + \gamma} \right] - \log(1 + \gamma) \right], \end{aligned}$$

which proves (11). To find the maxima over γ , we take the derivative with respect to γ :

$$\begin{aligned} \frac{1}{1 + \gamma} &= \bar{X}_S \frac{1}{(1 + \gamma)^2} \\ \Rightarrow 1 + \gamma &= \bar{X}_S. \end{aligned} \quad (47)$$

This equation will have a solution $\gamma \geq 0$ if and only if $\bar{X}_S \geq 1$. When $\bar{X}_S \geq 1$, the maximizing value is $\gamma = \bar{X}_S - 1$. Substituting this expression into (11), we obtain:

$$\begin{aligned} J(S) &= \max_{\gamma \geq 0} J(S, \gamma) \\ &= |S| \left[\bar{X}_S - 1 - \log(\bar{X}_S) \right] \text{ when } \bar{X}_S \geq 1. \end{aligned} \quad (48)$$

When $\bar{X}_S \leq 1$, the maximum value of $J(S, \gamma)$ occurs when $\gamma = 0$, in which case:

$$J(S) = 0 \text{ when } \bar{X}_S < 1. \quad (49)$$

The formula (13) matches (48) when $\bar{X}_S \geq 1$ (49) when $\bar{X}_S < 1$.

APPENDIX B PROOF OF LEMMA 2

The proof is a simple application of a union bound:

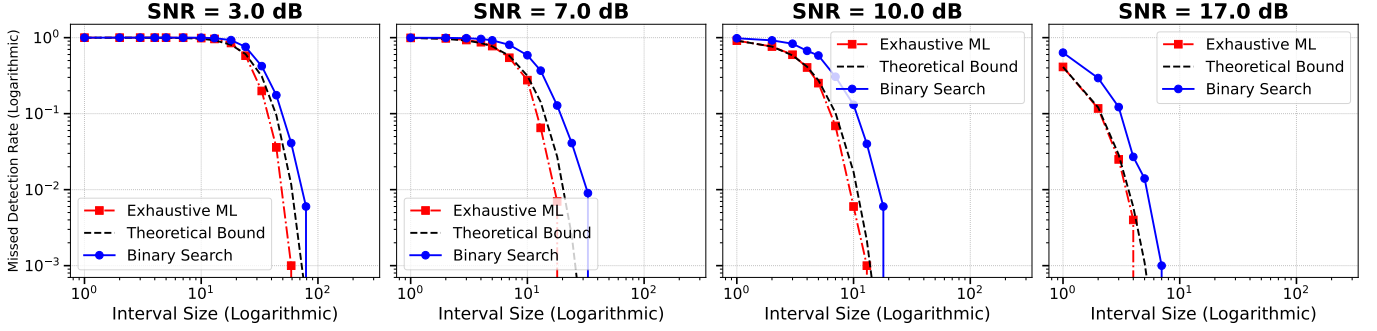
$$\begin{aligned} P_{FA} &= \mathbb{P} \left(\hat{H} = 1 | H = 0 \right) \\ &= \mathbb{P} \left(\bar{X}_S^+ \geq u_{|S|} \text{ for some } S | H = 0 \right) \\ &\leq \sum_S \mathbb{P} \left(\bar{X}_S^+ \geq u_{|S|} | H = 0 \right) \end{aligned} \quad (50)$$

Hence, we can approximate the bound (50) as:

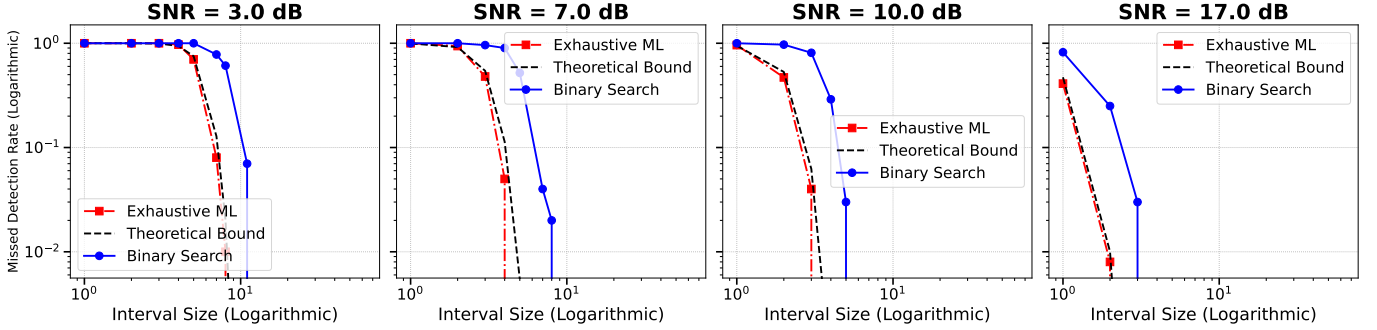
$$P_{FA} \leq \frac{N^2}{2} \max_S \mathbb{P} \left(\bar{X}_S^+ \geq u_{|S|} | H = 0 \right). \quad (51)$$

Also, from (12), we have that

$$|S| \bar{X}_S = \sum_{n \in S} X_n.$$



(a) The missed detection rate of maximum likelihood methods for different signal sizes (false alarm rate fixed at 10^{-6}) for the one-dimensional data.



(b) The missed detection rate of maximum likelihood methods for different signal sizes (false alarm rate fixed at 10^{-6}) for the two-dimensional data.

Fig. 8: The missed detection rate of the exhaustive and binary search maximum likelihood estimations and U-Net for 1D and 2D signals with sizes ranging from 1 to 256 (out of $N = 1024$) for 1D and 1 to 64 (out of $N = 128$) for 2D. Each plot represents the performance for a specific fixed signal SNR.

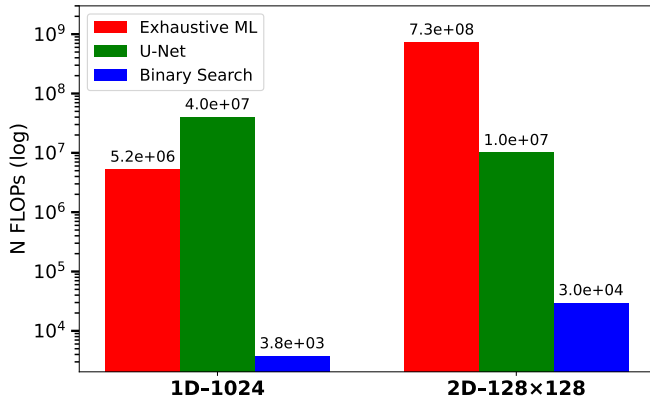


Fig. 9: Comparison of number of FLOPs needed for the proposed binary search method, exhaustive ML method, and U-Net for one-dimensional signals of size 1024 and two-dimensional signals of size 128×128 . The results indicate that the computational complexity of the proposed method is reduced by three to four orders of magnitude.

Under the null hypothesis, $H = 0$, the values X_n are i.i.d. exponential random variables with a mean $\mathbb{E}(X_n) = 1$. Thus,

$$Z_S := 2|S|\bar{X}_S$$

is a chi-squared random variable with $2|S|$ degrees of freedom [67]. Therefore, for any set S with $|S| = \ell$,

$$\begin{aligned} \mathbb{P}(\bar{X}_S^+ \geq u_{|S|} | H = 0) &= \mathbb{P}(\bar{X}_S^+ \geq u_\ell | H = 0) \\ &= \mathbb{P}(\bar{X}_S \geq u_\ell | H = 0) \\ &= \mathbb{P}(Z_S \geq 2\ell u_\ell | H = 0) = F(2\ell u_\ell; 2\ell). \end{aligned} \quad (52)$$

Substituting (52) into (51), we obtain (21).

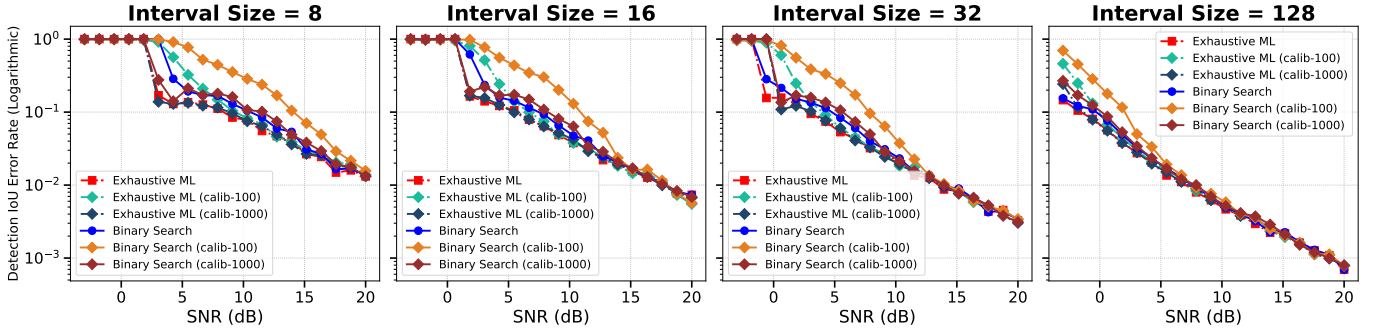
APPENDIX C PROOF OF LEMMA 3

Let S and γ be the true signal region and SNR under the signal present hypothesis $H = 1$. The probability of missed detection is:

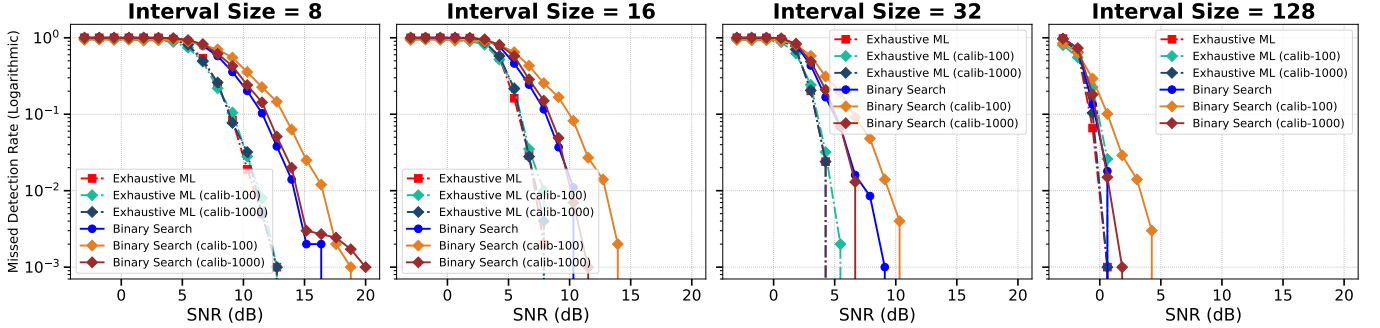
$$\begin{aligned} P_{\text{MD}} &= \mathbb{P}(\hat{H} = 0 | H = 1) \\ &= \mathbb{P}(\bar{X}_{S'} < u_{|S'|} \text{ for all } S') \\ &\leq \mathbb{P}(\bar{X}_S \leq u_{|S|}). \end{aligned} \quad (53)$$

That is, we can bound the missed detection probability by the behavior on the true set. Now, under the hypothesis $H = 1$, for all elements $n \in S$, X_n is exponentially distributed with $\mathbb{E}(X_n) = (1 + \gamma)$. Hence,

$$Z_S = 2|S|\bar{X}_S / (1 + \gamma)$$



(a) The detection IOU error rate of different methods for a range of SNRs (false alarm rate fixed at 10^{-6}) for the one-dimensional data.



(b) The missed detection rate of maximum likelihood methods for a range of SNRs (false alarm rate fixed at 10^{-6}) for the one-dimensional data.

Fig. 10: The detection IOU error rate and missed detection rate of the exhaustive and binary search maximum likelihood estimations for 1D signals across SNRs ranging from -3 to 20 dB. Each curve corresponds to a fixed signal size. Results are shown for both the ideal case with perfectly known noise variance and the non-ideal case where the noise power is estimated from N_{ref} calibration samples (N_{ref} is indicated within parentheses). Increasing N_{ref} reduces the estimation variance and improves detection performance, illustrating the trade-off between calibration overhead and detection reliability.

is chi-squared distributed with $2|S|$ degrees of freedom. Therefore, using the complementary CDF in (22), we can write the probability bound in (53) as

$$P_{\text{MD}} \leq 1 - F\left(\frac{2\ell u_\ell}{1 + \gamma}; 2\ell\right), \quad (54)$$

where $\ell = |S|$.

APPENDIX D PROOF OF THEOREM 4

A. Equivalent Algorithm

Before proving the theorem, we first rewrite Algorithm. 2 in the form of Algorithm. 3 which is easier to analyze. The following lemma shows that these two algorithms are equivalent; hence, we can focus on Algorithm. 3 for the subsequent analysis.

Lemma 5. Fix N and consider any power measurements X_n . Let

$$(\hat{a}_0^{(t)}, \hat{b}_0^{(t)}) = (\hat{a}^{(t)}, \hat{b}^{(t)}) \quad (55)$$

denote the estimates generated from Algorithm. 2, and let

$$(\hat{a}_1^{(t)}, \hat{b}_1^{(t)}) = (\hat{a}^{(t)}, \hat{b}^{(t)}) \quad (56)$$

be the outputs of Algorithm. 3 with input $Z_{m,i}$ in (33). Then, for all $t = 0, \dots, M - 1$:

$$(\hat{a}_1^{(t)}, \hat{b}_1^{(t)}) = (\hat{a}_0^{(t)}, \hat{b}_0^{(t)}). \quad (57)$$

Proof. We use induction for the proof. For $t = 0$, we have:

$$\begin{aligned} \hat{a}_0^{(0)} &= \hat{i}^{(0)} \ell_0 = 0, & \hat{b}_0^{(0)} &= \hat{j}^{(0)} \ell_0 = N, \\ \hat{a}_1^{(0)} &= 0, & \hat{b}_1^{(0)} &= N \end{aligned} \quad (58)$$

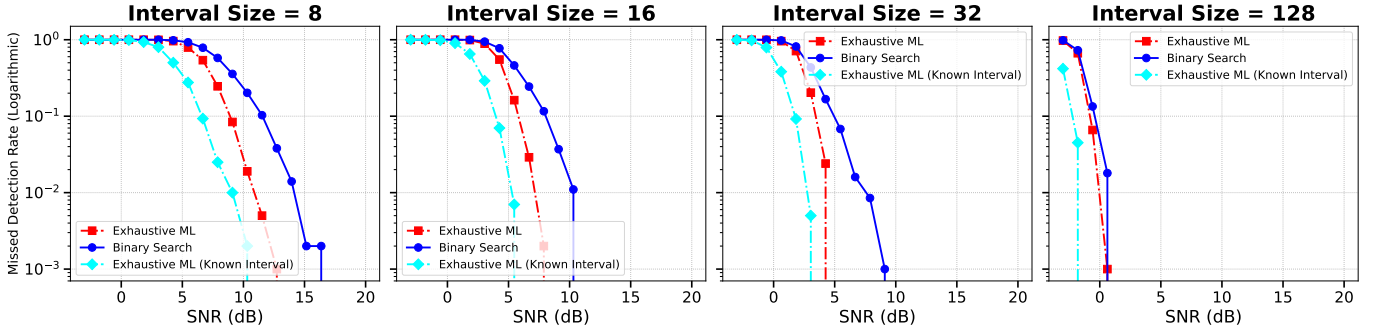
Suppose that the argument holds for step t , so we have:

$$(\hat{a}_1^{(t)}, \hat{b}_1^{(t)}) = (\hat{a}_0^{(t)}, \hat{b}_0^{(t)}). \quad (59)$$

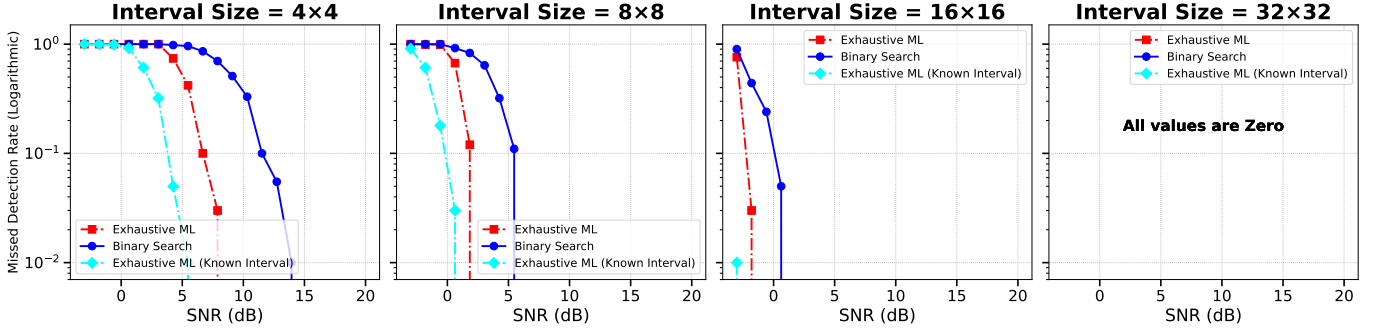
we intend to prove that it will also hold for step $t + 1$. We prove the equivalence of $\hat{a}_0^{(t+1)}$ and $\hat{a}_1^{(t+1)}$; for \hat{b} , it will be exactly the same.

$$\begin{aligned} \hat{a}_0^{(t+1)} &= \hat{i}^{(t+1)} \ell_{(t+1)} = (2\hat{i}^{(t)} + \delta_{\max}) \ell_{(t+1)} \\ \hat{a}_1^{(t+1)} &= \hat{a}_1^{(t)} + \delta_{\max} \ell_{(t+1)} \end{aligned} \quad (60)$$

where δ_{\max} is the δ that maximizes the objective function J' , which is exactly the same for both algorithms. But by assumption, we know that $\hat{a}_1^{(t)} = \hat{a}_0^{(t)}$, and by Algorithm 2, we also know that $\hat{a}_0^{(t)} = \hat{i}^{(t)} \ell_t$ and $\ell_{(t+1)} = 2\ell_t$. So we'll



(a) The missed detection rate of maximum likelihood methods for different SNRs (false alarm rate fixed at 10^{-6}) for the one-dimensional data.



(b) The missed detection rate of maximum likelihood methods for different SNRs (false alarm rate fixed at 10^{-6}) for the two-dimensional data.

Fig. 11: The missed detection rate of the exhaustive and binary search detectors, for 1D and 2D signal cases across SNRs ranging from -3 dB to 20 dB. Each subplot corresponds to a fixed signal interval size ℓ_0 . The oracle (known interval) benchmark illustrates the lower bound on the missed detection rate achievable when the true signal interval is known. The results highlight the degradation introduced by interval uncertainty.

have:

$$\begin{aligned}\hat{a}_1^{(t+1)} &= \hat{a}_1^{(t)} + \delta_{max} \ell_{(t+1)} = \hat{i}^{(t)} 2\ell_{(t+1)} + \delta_{max} \ell_{(t+1)} \\ &= (2\hat{i}^{(t)} + \delta_{max}) \ell_{(t+1)} = \hat{a}_0^{(t+1)}\end{aligned}\quad (61)$$

which proves the equivalency of $\hat{\alpha}_0$ and $\hat{\alpha}_1$. The equivalency of $\hat{\beta}_0$ and $\hat{\beta}_1$ could be proved exactly with the same logic. \square

B. Asymptotic Likelihood Function

In this subsection, we derive a simple expression for the likelihood function in the limit of large N . The likelihood function (13) implicitly depends on N . To make this dependence explicit, we will write $J_N(S)$ for $J(S)$ where the set $S \subseteq \{0, 1, \dots, N-1\}$. Next, for any α, β with

$$0 \leq \alpha \leq \beta \leq 1, \quad (62)$$

we define the sequences

$$a_N = \lfloor \alpha N \rfloor, \quad b_N = \lfloor \beta N \rfloor, \quad (63)$$

and let S_N denote the interval

$$S_N = [a_N, b_N]. \quad (64)$$

Note that, by the definition of (40), S_N^0 is S_N for $\alpha = \alpha^0$ and $\beta = \beta^0$. Also, define the function:

$$G_N(\alpha, \beta) := \frac{1}{N} J_N(\lfloor \alpha N \rfloor, \lfloor \beta N \rfloor), \quad (65)$$

which represents a normalized version of the likelihood function on the interval S_N .

Lemma 6. For any α and β satisfying (62) and

$$\alpha \leq \beta^0 \text{ and } \beta \geq \alpha^0, \quad (66)$$

we have that:

$$\lim_{N \rightarrow \infty} \overline{X}_{S_N} = Z(\alpha, \beta), \quad (67)$$

$$\lim_{N \rightarrow \infty} G_N(\alpha, \beta) = G(\alpha, \beta) \quad (68)$$

where the convergence is almost surely and

$$Z(\alpha, \beta) := 1 + \gamma \frac{\min\{\beta^0, \beta\} - \max\{\alpha_0, \alpha\}}{\beta - \alpha} \quad (69)$$

$$G(\alpha, \beta) := (\beta - \alpha) [Z(\alpha, \beta) - 1 - \log Z(\alpha, \beta)] \quad (70)$$

Proof. For any S , \overline{X}_S in (12) is the average of values X_n with $n \in S$. Therefore, the expected values in (1) show that

$$\mathbb{E}(\overline{X}_S) = 1 + \frac{|S \cap S_N^0|}{|S|} \gamma. \quad (71)$$

Algorithm 3 Equivalent Binary Interval Estimation

Require: Interval length $N = 2^M$
Require: Dyadic powers $Z_{m,i}$

```

1:  $\hat{a}^{(0)} \leftarrow 0, \hat{b}^{(0)} \leftarrow N$ 
2:  $J_{\max} = J([\hat{a}^{(0)}, \hat{b}^{(0)}])$ 
3:  $\ell_0 \leftarrow 2^M$  // initial sub-interval length
4: for  $t = 0, \dots, M - 1$  do
5:   // Get layer info
6:    $m \leftarrow M - t - 1$  // layer
7:    $\ell_{t+1} \leftarrow 2^m$  // sub-interval length
8:
9:   // Optimization over the left boundary
10:   $\hat{a}^{(t+1)} \leftarrow \hat{a}^{(t)}$ 
11:  for  $\delta \in \{-1, 1\}$  do
12:     $a' \leftarrow \hat{a}^{(t)} + \delta \ell_{t+1}$ 
13:     $S' = [a', \hat{b}^{(t)})$ 
14:     $J' \leftarrow J(S')$ 
15:    if  $J' > J_{\max}, |S'| > 0$ , and  $a' \geq 0$  then
16:       $J_{\max} \leftarrow J'$ 
17:       $\hat{a}^{(t+1)} \leftarrow a'$ 
18:    end if
19:  end for
20:
21:  // Optimization over the right boundary
22:   $\hat{b}^{(t+1)} \leftarrow \hat{b}^{(t)}$ 
23:  for  $\delta \in \{-1, 1\}$  do
24:     $b' \leftarrow \hat{b}^{(t)} + \delta \ell_{t+1}$ 
25:     $S' = [\hat{a}^{(t+1)}, b')$ 
26:     $J' \leftarrow J(S')$ 
27:    if  $J' > J_{\max}, |S'| > 0$ , and  $b' \leq N$  then
28:       $J_{\max} \leftarrow J'$ 
29:       $\hat{b}^{(t+1)} \leftarrow b'$ 
30:    end if
31:  end for
32: end for

```

From the definitions of S_N^0 in (40) and S_N in (63) and (64), as well as the condition (66), we have that

$$\lim_{N \rightarrow \infty} \frac{|S_N \cap S_N^0|}{N} = \min\{\beta_0, \beta\} - \max\{\alpha_0, \alpha\} \quad (72a)$$

$$\lim_{N \rightarrow \infty} \frac{|S_N|}{N} = \beta - \alpha. \quad (72b)$$

Also, since \bar{X}_{S_N} is an average of i.i.d. random variables, it follows from the strong law of large numbers that

$$\begin{aligned} \lim_{N \rightarrow \infty} \bar{X}_{S_N} &= \lim_{N \rightarrow \infty} \mathbb{E}(\bar{X}_{S_N}) \\ &= 1 + \gamma \lim_{N \rightarrow \infty} \frac{|S \cap S_N^0|}{|S|} \\ &= 1 + \gamma \frac{\min\{\beta_0, \beta\} - \max\{\alpha_0, \alpha\}}{\beta - \alpha} \\ &= Z(\alpha, \beta), \end{aligned} \quad (73)$$

which proves (67). From (65) and (13) we have that:

$$\begin{aligned} G_N(\alpha, \beta) &= \frac{1}{N} J_N([\alpha N], [\beta N]) \\ &= \frac{[\beta N] - [\alpha N]}{N} [\bar{X}_{S_N} - 1 - \log(\bar{X}_{S_N})] \end{aligned} \quad (74)$$

From (67), this limit is given by:

$$\begin{aligned} \lim_{N \rightarrow \infty} G_N(\alpha, \beta) &= (\beta - \alpha) [Z(\alpha, \beta) - 1 - \log Z(\alpha, \beta)] \\ &= G(\alpha, \beta) \end{aligned} \quad (75)$$

which proves (68). \square

We will call the function $G(\alpha, \beta)$ the *asymptotic normalized likelihood* and $Z(\alpha, \beta)$ the *asymptotic average signal energy*. An important property of the asymptotic normalized likelihood function is that it possesses a certain *triangular maximization* property, as given by the following definition.

Definition 7. A scalar-valued function $f(x)$ of a scalar x in some interval A has a *triangular maxima* at $x = x^*$ with constant $c > 0$ if:

- (a) $f'(x) > c$ in the region $x < x^*$ and $x \in A$.
- (b) $f'(x) < -c$ in the region $x > x^*$ and $x \in A$.

Note that if x^* is a triangular maxima in an interval A , then $x^* = \operatorname{argmax} f(x)$ for $x \in A$.

Lemma 8. Fix any $\alpha_0 < \beta_0$ and γ , and consider the asymptotic normalized likelihood function $G(\alpha, \beta)$ in (70). There exists a constant c , possibly dependent on γ , such that:

- (a) For fixed $\alpha \leq \beta^0$, $G(\alpha, \beta)$ has a triangular maximum at $\beta = \beta^0$ with constant c in the region $\beta \geq \alpha^0$.
- (b) For fixed $\beta \geq \alpha^0$, $G(\alpha, \beta)$ has a triangular maximum at $\alpha = \alpha^0$ with constant c in the region $\alpha \leq \beta^0$.

Proof. We prove the first part with a fixed α ; the second part can be proved similarly. We can write $Z(\alpha, \beta)$ as:

$$Z(\alpha, \beta) = \begin{cases} 1 + \gamma \frac{\beta_0 - \hat{\alpha}}{\beta - \hat{\alpha}}, & \text{if } \beta \geq \beta_0 \\ 1 + \gamma \frac{\beta - \hat{\alpha}}{\beta - \alpha}, & \text{if } \beta < \beta_0 \end{cases} \quad (76)$$

where $\hat{\alpha} = \max\{\alpha, \alpha^0\}$. So the derivatives of Z with respect to β will be:

$$\frac{\partial Z}{\partial \beta} = \begin{cases} -\gamma \frac{\beta_0 - \hat{\alpha}}{(\beta - \hat{\alpha})^2}, & \text{if } \beta \geq \beta_0 \\ \gamma \frac{\beta - \hat{\alpha}}{(\beta - \alpha)^2}, & \text{if } \beta < \beta_0 \end{cases} \quad (77)$$

On the other hand, according to (70), we can write the partial derivatives of G as:

$$\frac{\partial G}{\partial \beta} = Z(\beta) - 1 - \log Z(\beta) + (\beta - \alpha) \frac{\partial Z}{\partial \beta} \left[1 - \frac{1}{Z(\beta)} \right] \quad (78)$$

From (76) and (77) we have:

$$\frac{\partial G}{\partial \beta} = \begin{cases} f_1(Z), & \text{if } \beta \geq \beta_0 \\ f_2(Z, \beta), & \text{if } \beta < \beta_0 \end{cases} \quad (79)$$

where:

$$\begin{aligned} f_1(Z) &= -\log(Z) + 1 - \frac{1}{Z} \\ f_2(Z, \beta) &= Z - 1 - \log(Z) + \gamma \frac{\hat{\alpha} - \alpha}{\beta - \alpha} \left[1 - \frac{1}{Z} \right] \end{aligned} \quad (80)$$

We can rewrite $f_1(Z)$ as:

$$f_1(Z) = \log\left(\frac{1}{Z}\right) + 1 - \frac{1}{Z} = -\left[\frac{1}{Z} - 1 - \log\left(\frac{1}{Z}\right)\right] \quad (81)$$

From (70), we know that $Z > 1 + \epsilon$ for some $\epsilon > 0$, and all β . We also know that $s(t) = t - 1 - \log(t)$ is always positive and only zero at $t = 1$. Hence, there is a constant $c > 0$ such that $f_1(Z) < -c$ for all $z \geq 1 + \epsilon$. So,

$$\frac{\partial G}{\partial \beta} < -c \text{ for } \beta > \beta_0. \quad (82)$$

For the region $\beta \in [\alpha^0, \beta^0]$, we can break $f_2(Z, \beta)$ into two parts: $f_2^1(Z)$ and $f_2^2(Z, \beta)$, where:

$$f_2^1(Z) = Z - 1 - \log(Z) \quad (83)$$

$$f_2^2(Z, \beta) = \gamma \frac{\hat{\alpha} - \alpha}{\beta - \alpha} \left[1 - \frac{1}{Z}\right]. \quad (84)$$

We have $f_2^2(Z, \beta) \geq 0$ since $\hat{\alpha} = \max\{\alpha_0, \alpha\}$ and $Z > 1$. Also, similarly to above, we can show that $f_2^1(Z) > c$ for some c and all $Z = Z(\alpha, \beta)$ with $\beta \in [\alpha^0, \beta^0]$. Therefore,

$$\frac{\partial G}{\partial \beta} > c \text{ for } \beta < \beta_0. \quad (85)$$

□

C. Proof of Theorem 4

To make the dependence on N explicit, let $\hat{a}_N^{(t)}$ and $\hat{b}_N^{(t)}$ be the outputs of the equivalent algorithm, Algorithm 3, with the input size N . Let $\hat{\alpha}_N^{(t)}$ and $\hat{\beta}_N^{(t)}$ be the normalized values

$$\hat{\alpha}_N^{(t)} = \frac{\hat{a}_N^{(t)}}{N}, \quad \hat{\beta}_N^{(t)} = \frac{\hat{b}_N^{(t)}}{N}. \quad (86)$$

Since $\hat{a}_N^{(t)}$ and $\hat{b}_N^{(t)}$ are integer multiples of $\ell_t = N2^{-t}$, the normalized estimates $\hat{\alpha}^{(t)}$ and $\hat{\beta}^{(t)}$ will be at the discrete points:

$$\hat{\alpha}^{(t)} = \hat{i}^{(t)}2^{-t}, \quad \hat{\beta}^{(t)} = \hat{j}^{(t)}2^{-t}, \quad (87)$$

for some integer indices

$$\hat{i}^{(t)}, \hat{j}^{(t)} = 0, \dots, 2^t. \quad (88)$$

Now fix any $t_0 \geq 0$. Since there are at most a finite number of choices in (88), Lemma 6 shows that, with probability one, there exists an N_0 such that

$$|G_N(i2^{-t}, j2^{-t}) - G(i2^{-t}, j2^{-t})| < c2^{-t-2}, \quad (89)$$

where c is the constant in Lemma 8, and all the inequalities are valid for all $i, j = 0, \dots, 2^t$, $N \geq N_0$, and $t \leq t_0$. We are now ready to prove our main induction step.

Lemma 9. *Let t_0 and N_0 be defined as above. With probability one, for all $N \geq N_0$ and $t \leq t_0$, $\hat{\alpha}_N^{(t)}$ and $\hat{\beta}_N^{(t)}$ have a bounded distance from the true values α^0 and β^0 in the sense that:*

$$|\hat{\alpha}_N^{(t)} - \alpha^0| \leq \delta_t, \quad |\hat{\beta}_N^{(t)} - \beta^0| \leq \delta_t \quad (90)$$

where $\delta_t = 2^{-t}$.

Proof. We use induction for the proof. For $t = 0$ we will have:

$$|\hat{\alpha}^{(0)} - \alpha_0| \leq 1, \quad |\hat{\beta}^{(0)} - \beta_0| \leq 1 \quad (91)$$

since all values are in the interval $[0, 1]$ and thus their distance cannot be larger than 1. Suppose (90) holds for the t -th step with $t < t_0$. We prove that (90) also holds for step $t + 1$. The optimization over the left boundary in Algorithm. 3 is equivalent to

$$\hat{\alpha}_N^{(t+1)} = \operatorname{argmax}_a J_N([a, \hat{b}_N^{(t)}]), \quad (92)$$

$$\text{s.t. } a = \hat{a}_N^{(t)} + \{0, \pm \ell_{t+1}\}. \quad (93)$$

Since $\ell_{t+1} = \delta_{t+1}N$, (86) and (65) show that the maximization can be re-written as:

$$\hat{\alpha}_N^{(t+1)} = \operatorname{argmax}_\alpha G_N(\alpha, \hat{\beta}_N^{(t)})$$

$$\text{s.t. } \hat{\alpha}_N^{(t+1)} = \hat{\alpha}_N^{(t)} + \{0, \pm \delta_{t+1}\}. \quad (94)$$

Now define

$$\alpha_N^{(t+1)} = \operatorname{argmax}_\alpha G(\alpha, \hat{\beta}_N^{(t)})$$

$$\text{s.t. } \alpha_N^{(t+1)} = \hat{\alpha}_N^{(t)} + \{0, \pm \delta_{t+1}\}, \quad (95)$$

which is identical to $\hat{\alpha}_N^{(t+1)}$, except that we have replaced $G_N(\cdot)$ in the objective function with $G(\cdot)$, its asymptotic limit. So, there are three possibilities for $\alpha_N^{(t+1)}$. We will show that

$$|\hat{\alpha}_N^{(t+1)} - \alpha^0| \leq \delta_{t+1} \quad (96)$$

for all three cases.

Case 1: $\alpha_N^{(t+1)} = \hat{\alpha}_N^{(t)}$. In this case, we know that

$$G(\hat{\alpha}_N^{(t)}, \hat{\beta}_N^{(t)}) \geq G(\hat{\alpha}_N^{(t)} - \delta_{t+1}, \hat{\beta}_N^{(t)}) \quad (97a)$$

$$G(\hat{\alpha}_N^{(t)}, \hat{\beta}_N^{(t)}) \geq G(\hat{\alpha}_N^{(t)} + \delta_{t+1}, \hat{\beta}_N^{(t)}) \quad (97b)$$

Since $G(\alpha, \hat{\beta}_N^{(t)})$ has a triangular maximum at $\alpha = \alpha^0$ it must be that α^0 is in the interval

$$\alpha^0 \in [\hat{\alpha}_N^{(t)} - \delta_{t+1}, \hat{\alpha}_N^{(t)} + \delta_{t+1}]. \quad (98)$$

Hence either:

$$\alpha^0 \in [\hat{\alpha}_N^{(t)} - \delta_{t+1}, \hat{\alpha}_N^{(t)}] \quad (99)$$

or

$$\alpha^0 \in [\hat{\alpha}_N^{(t)}, \hat{\alpha}_N^{(t)} + \delta_{t+1}]. \quad (100)$$

WLOG assume α^0 is in the interval (99). Therefore,

$$\begin{aligned} & G_N(\hat{\alpha}_N^{(t+1)} + \delta_{t+1}, \hat{\beta}_N^{(t)}) \\ & \stackrel{(a)}{<} G(\hat{\alpha}_N^{(t+1)} + \delta_{t+1}, \hat{\beta}_N^{(t)}) + \frac{c}{2}\delta_{t+1} \\ & \stackrel{(b)}{\leq} G(\hat{\alpha}_N^{(t+1)}, \hat{\beta}_N^{(t)}) + \frac{c}{2}\delta_{t+1} - c\delta_{t+1} \\ & \stackrel{(c)}{<} G_N(\hat{\alpha}_N^{(t+1)}, \hat{\beta}_N^{(t)}) - \frac{c}{2}\delta_{t+1} + \frac{c}{2}\delta_{t+1} \\ & \leq G_N(\hat{\alpha}_N^{(t+1)}, \hat{\beta}_N^{(t)}) \end{aligned} \quad (101)$$

where (a) is due to (89); (b) is due the fact that $G(\alpha, \beta)$ has a triangular maxima at $\alpha^0 \leq \hat{\alpha}_N^{(t)}$; and (c) again is due to (89). Hence in the maximization (94), we have that either $\hat{\alpha}_N^{(t+1)}$

satisfies

$$\widehat{\alpha}^{(t+1)} \in \{\widehat{\alpha}^{(t)} - \delta_{t+1}, \widehat{\alpha}^{(t)}\}. \quad (102)$$

Since by assumption α^0 is in the interval (99), it follows that (96) holds.

Case 2: $\alpha_N^{(t+1)} = \widehat{\alpha}_N^{(t)} + \delta_{t+1}$. In this case, we know that

$$G(\widehat{\alpha}_N^{(t)} + \delta_{t+1}, \widehat{\beta}_N^{(t)}) \geq G(\widehat{\alpha}_N^{(t)} - \delta_{t+1}, \widehat{\beta}_N^{(t)}) \quad (103a)$$

$$G(\widehat{\alpha}_N^{(t)} + \delta_{t+1}, \widehat{\beta}_N^{(t)}) \geq G(\widehat{\alpha}_N^{(t)}, \widehat{\beta}_N^{(t)}). \quad (103b)$$

Since $G(\alpha, \widehat{\beta}_N^{(t)})$ has a triangular maximum at $\alpha = \alpha^0$, it must be $\alpha^0 \geq \widehat{\alpha}_N^{(t)}$. Also, by the induction hypothesis, $\alpha^0 \leq \widehat{\alpha}_N^{(t)} - \delta_t$. Hence, α^0 is in the interval:

$$\alpha^0 \in [\widehat{\alpha}_N^{(t)}, \widehat{\alpha}_N^{(t)} + \delta_t]. \quad (104)$$

In particular, since $\delta_{t+1} = \delta_t/2$, either:

$$\alpha^0 \in [\widehat{\alpha}_N^{(t)}, \widehat{\alpha}_N^{(t)} + \delta_{t+1}] \quad (105)$$

or

$$\alpha^0 \in [\widehat{\alpha}_N^{(t)} + \delta_{t+1}, \widehat{\alpha}_N^{(t)} + 2\delta_{t+1}]. \quad (106)$$

Suppose that α^0 is in the interval (105). Then, a similar argument as (101) shows that

$$G_N(\widehat{\alpha}_N^{(t+1)} - \delta_{t+1}, \widehat{\beta}_N^{(t)}) \leq G_N(\widehat{\alpha}_N^{(t+1)}, \widehat{\beta}_N^{(t)}) \quad (107)$$

which shows that $\widehat{\alpha}_N^{(t)}$ must be one of the two values:

$$\widehat{\alpha}^{(t+1)} \in \{\widehat{\alpha}^{(t)}, \widehat{\alpha}^{(t)} + \delta_{t+1}\}. \quad (108)$$

Since α^0 is the interval (105) we see that (96) is satisfied. Similarly, if α^0 is in the interval (106), one can show that

$$G_N(\widehat{\alpha}_N^{(t+1)}, \widehat{\beta}_N^{(t)}) \leq G_N(\widehat{\alpha}_N^{(t+1)} + \delta_{t+1}, \widehat{\beta}_N^{(t)}), \quad (109)$$

which shows that $\widehat{\alpha}_N^{(t)}$ must be one of the two values:

$$\widehat{\alpha}^{(t+1)} \in \{\widehat{\alpha}^{(t)} + \delta_{t+1}, \widehat{\alpha}^{(t)} + 2\delta_{t+1}\}. \quad (110)$$

Since α^0 is the interval (106) we see that (96) is satisfied.

Case 3: $\alpha_N^{(t+1)} = \widehat{\alpha}_N^{(t)} + \delta_{t+1}$. Similarly to case 2, we can show that (96) is satisfied.

Hence, we have shown that, in all three cases (96) is satisfied. The proof for $|\widehat{\beta}_N^{(t+1)} - \beta^0| \leq \delta_{t+1}$ is similar. So, by induction, (90) is satisfied for all $N \geq N_0$ and $t \leq t_0$ with probability one. \square

Now we proceed to prove (43). We have:

$$\text{IoU}_N^{(t)} = \frac{|\widehat{S}_N^{(t)} \cap S_N^0|}{|\widehat{S}_N^{(t)} \cup S_N^0|} \quad (111)$$

On the other hand, we have:

$$\begin{aligned} S_N^0 &= [a_N^0, b_N^0], \quad a_N^0 = \lfloor \alpha_0 N \rfloor, \quad b_N^0 = \lfloor \beta_0 N \rfloor, \\ \widehat{S}_N^{(t)} &= [\widehat{a}_N^{(t)}, \widehat{b}_N^{(t)}], \quad a_N^{(t)} = \widehat{a}_N^{(t)} N, \quad b_N^{(t)} = \widehat{b}_N^{(t)} N \end{aligned} \quad (112)$$

So, at the limit, we'll have:

$$\lim_{N \rightarrow \infty} \text{IoU}_N^{(t)} = \lim_{N \rightarrow \infty} \frac{|\min(\widehat{\beta}_N^{(t)}, \beta_0) - \max(\widehat{\alpha}_N^{(t)}, \alpha_0)|}{|\max(\widehat{\beta}_N^{(t)}, \beta_0) - \min(\widehat{\alpha}_N^{(t)}, \alpha_0)|} \quad (113)$$

Lemma 9 and the triangle inequality show:

$$\begin{aligned} \lim_{N \rightarrow \infty} \min\{|\widehat{\beta}^{(t)}, \beta_0\} &\geq \beta^0 - |\widehat{\beta}^{(t)} - \beta^0| \geq \beta^0 - 2^{-t} \\ \lim_{N \rightarrow \infty} \max\{|\widehat{\beta}^{(t)}, \beta_0\} &\leq \beta^0 + |\widehat{\beta}^{(t)} - \beta_0| \leq \beta^0 - 2^{-t} \\ \lim_{N \rightarrow \infty} \min\{|\widehat{\alpha}^{(t)}, \alpha\} &\geq \beta^0 - |\widehat{\alpha}^{(t)} - \alpha^0| \geq \beta^0 - 2^{-t} \\ \lim_{N \rightarrow \infty} \max\{|\widehat{\alpha}^{(t)}, \alpha\} &\leq \alpha^0 + |\widehat{\alpha}^{(t)} - \alpha| \leq \alpha^0 - 2^{-t}. \end{aligned}$$

Since the nominator and denominator of the IoU in (113) are positive, we can bound its limit as follows:

$$\begin{aligned} \lim_{N \rightarrow \infty} \text{IoU}_N^{(t)} &\geq \frac{|\beta_0 - \alpha_0| - 2^{-(t+1)}}{|\beta_0 - \alpha_0| + 2^{-(t+1)}} \\ &= 1 - \frac{2^{-(t+2)}}{|\beta_0 - \alpha_0| + 2^{-(t+1)}} \geq 1 - \frac{2^{-(t+2)}}{\beta_0 - \alpha_0}, \end{aligned} \quad (114)$$

where the limit is true almost surely for any fixed t . Since there are a countable number of values of t , it follows that

$$\lim_{N, t \rightarrow \infty} \text{IoU}_N^{(t)} = 1 \quad (115)$$

almost surely, which proves (4).

REFERENCES

- [1] A. Ali and W. Hamouda, "Advances on spectrum sensing for cognitive radio networks: Theory and applications," *IEEE communications surveys & tutorials*, vol. 19, no. 2, pp. 1277–1304, 2016.
- [2] T. Yucek and H. Arslan, "A survey of spectrum sensing algorithms for cognitive radio applications," *IEEE communications surveys & tutorials*, vol. 11, no. 1, pp. 116–130, 2009.
- [3] A. Nasser, H. Al Haj Hassan, J. Abou Chaaya, A. Mansour, and K.-C. Yao, "Spectrum sensing for cognitive radio: Recent advances and future challenge," *Sensors*, vol. 21, no. 7, p. 2408, 2021.
- [4] D. Janu, K. Singh, and S. Kumar, "Machine learning for cooperative spectrum sensing and sharing: A survey," *Transactions on Emerging Telecommunications Technologies*, vol. 33, no. 1, p. e4352, 2022.
- [5] K.-G. Lee and S.-J. Oh, "Detection of frequency-hopping signals with deep learning," *IEEE Communications Letters*, vol. 24, no. 5, pp. 1042–1046, 2020.
- [6] M. Lin, X. Zhang, Y. Tian, and Y. Huang, "Multi-signal detection framework: A deep learning based carrier frequency and bandwidth estimation," *Sensors*, vol. 22, no. 10, p. 3909, 2022.
- [7] A. Gkelias and K. K. Leung, "Gan-based detection of adversarial em signal waveforms," in *MILCOM 2022-2022 IEEE Military Communications Conference (MILCOM)*. IEEE, 2022, pp. 356–361.
- [8] S. Kang, M. Mezzavilla, S. Rangan, A. Madanayake, S. B. Venkatakrishnan, G. Hellbourg, M. Ghosh, H. Rahmani, and A. Dhananjay, "Cellular wireless networks in the upper mid-band," *IEEE Open Journal of the Communications Society*, 2024.
- [9] S. Kang, G. Geraci, M. Mezzavilla, and S. Rangan, "Terrestrial-satellite spectrum sharing in the upper mid-band with interference nulling," in *ICC 2024-IEEE International Conference on Communications*. IEEE, 2024, pp. 5057–5062.
- [10] E. Soltanmohammadi, M. Orooji, and M. Naraghi-Pour, "Spectrum sensing over mimo channels using generalized likelihood ratio tests," *IEEE Signal Processing Letters*, vol. 20, no. 5, pp. 439–442, 2013.
- [11] L. Li, S. Hou, and A. L. Anderson, "Kernelized generalized likelihood ratio test for spectrum sensing in cognitive radio," *IEEE Transactions on Vehicular Technology*, vol. 67, no. 8, pp. 6761–6773, 2018.
- [12] K. S. V. Prasad, K. B. D'souza, and V. K. Bhargava, "A downscaled faster-RCNN framework for signal detection and time-frequency localization in wideband RF systems," *IEEE Transactions on Wireless Communications*, vol. 19, no. 7, pp. 4847–4862, 2020.
- [13] M. Tao, S. Tang, J. Li, X. Zhang, Y. Fan, and J. Su, "Radio frequency interference detection for sar data using spectrogram-based semantic network," in *2021 IEEE International Geoscience and Remote Sensing Symposium IGARSS*. IEEE, 2021, pp. 1662–1665.

- [14] A. Vagollari, V. Schram, W. Wicke, M. Hirschbeck, and W. Gerstacker, "Joint detection and classification of rf signals using deep learning," in *2021 IEEE 93rd Vehicular Technology Conference (VTC2021-Spring)*. IEEE, 2021, pp. 1–7.
- [15] W. Li, K. Wang, L. You, and Z. Huang, "A new deep learning framework for hf signal detection in wideband spectrogram," *IEEE Signal Processing Letters*, vol. 29, pp. 1342–1346, 2022.
- [16] S. Benazzouza, M. Ridouani, F. Salahdine, and A. Hayar, "A novel spectrogram based lightweight deep learning for iot spectrum monitoring," *Physical Communication*, vol. 64, p. 102364, 2024.
- [17] Z. Zhang, J. An, N. Ye, D. Niyato, and K. Yang, "Prompting and tuning: In-band interference segmentation using segment anything model," *IEEE Wireless Communications Letters*, 2024.
- [18] H. Urkowitz, "Energy detection of unknown deterministic signals," *Proceedings of the IEEE*, vol. 55, no. 4, pp. 523–531, 2005.
- [19] A. Margoosian, J. Abouei, and K. N. Plataniotis, "An accurate kernelized energy detection in gaussian and non-gaussian/impulsive noises," *IEEE Transactions on Signal Processing*, vol. 63, no. 21, pp. 5621–5636, 2015.
- [20] I. Sobron, P. S. Diniz, W. A. Martins, and M. Velez, "Energy detection technique for adaptive spectrum sensing," *IEEE Transactions on Communications*, vol. 63, no. 3, pp. 617–627, 2015.
- [21] E. Chatziantoniou, B. Allen, and V. Velisavljevic, "Threshold optimization for energy detection-based spectrum sensing over hyper-rayleigh fading channels," *IEEE Communications Letters*, vol. 19, no. 6, pp. 1077–1080, 2015.
- [22] R. Umar, A. U. Sheikh, and M. Deriche, "Unveiling the hidden assumptions of energy detector based spectrum sensing for cognitive radios," *IEEE communications surveys & tutorials*, vol. 16, no. 2, pp. 713–728, 2013.
- [23] L. Ma, Y. Li, and A. Demir, "Matched filtering assisted energy detection for sensing weak primary user signals," in *2012 IEEE International Conference on Acoustics, Speech and Signal Processing (ICASSP)*. IEEE, 2012, pp. 3149–3152.
- [24] X. Zhang, R. Chai, and F. Gao, "Matched filter based spectrum sensing and power level detection for cognitive radio network," in *2014 IEEE global conference on signal and information processing (GlobalSIP)*. IEEE, 2014, pp. 1267–1270.
- [25] S. Chaudhari, V. Koivunen, and H. V. Poor, "Autocorrelation-based decentralized sequential detection of ofdm signals in cognitive radios," *IEEE Transactions on Signal Processing*, vol. 57, no. 7, pp. 2690–2700, 2009.
- [26] G. Huang and J. K. Tugnait, "On cyclostationarity based spectrum sensing under uncertain gaussian noise," *IEEE Transactions on Signal Processing*, vol. 61, no. 8, pp. 2042–2054, 2013.
- [27] E. Rebeiz, P. Urriza, and D. Cabric, "Optimizing wideband cyclostationary spectrum sensing under receiver impairments," *IEEE Transactions on signal processing*, vol. 61, no. 15, pp. 3931–3943, 2013.
- [28] Y. Zeng and Y.-C. Liang, "Eigenvalue-based spectrum sensing algorithms for cognitive radio," *IEEE transactions on communications*, vol. 57, no. 6, pp. 1784–1793, 2009.
- [29] Z. Quan, S. Cui, A. H. Sayed, and H. V. Poor, "Optimal multiband joint detection for spectrum sensing in cognitive radio networks," *IEEE transactions on signal processing*, vol. 57, no. 3, pp. 1128–1140, 2008.
- [30] B. Farhang-Boroujeny, "Filter bank spectrum sensing for cognitive radios," *IEEE Transactions on signal processing*, vol. 56, no. 5, pp. 1801–1811, 2008.
- [31] M. Lin, A. P. Vinod, and C.-M. Samson, "Progressive decimation filter banks for variable resolution spectrum sensing in cognitive radios," in *2010 17th International Conference on Telecommunications*. IEEE, 2010, pp. 857–863.
- [32] S. E. El-Khany, M. S. El-Mahallawy, and E.-N. S. Youssef, "Improved wideband spectrum sensing techniques using wavelet-based edge detection for cognitive radio," in *2013 international conference on computing, networking and communications (ICNC)*. IEEE, 2013, pp. 418–423.
- [33] S. Jindal, D. Dass, and R. Gangopadhyay, "Wavelet based spectrum sensing in a multipath rayleigh fading channel," in *2014 Twentieth national conference on communications (NCC)*. IEEE, 2014, pp. 1–6.
- [34] M. Martone, "Multiresolution sequence detection in rapidly fading channels based on focused wavelet decompositions," *IEEE Transactions on Communications*, vol. 49, no. 8, pp. 1388–1401, 2002.
- [35] Z. Mohammadi and A. Zaimbashi, "Parallel multiband spectrum sensing in lte-based cognitive radios," *IEEE Transactions on Vehicular Technology*, vol. 73, no. 9, pp. 13 193–13 205, 2024.
- [36] A. Kumar and H. Sharma, "Intelligent cognitive radio spectrum sensing based on energy detection for advanced waveforms," *Radioelectronics and Communications Systems*, vol. 65, no. 3, pp. 149–154, 2022.
- [37] C. Vlădeanu, O. M. K. Al-Dulaimi, A. Marțian, and D. C. Popescu, "Average energy detection with adaptive threshold for spectrum sensing in cognitive radio systems," *IEEE Transactions on Vehicular Technology*, 2024.
- [38] Z. Tian and G. B. Giannakis, "A wavelet approach to wideband spectrum sensing for cognitive radios," in *2006 1st international conference on cognitive radio oriented wireless networks and communications*. IEEE, 2006, pp. 1–5.
- [39] S. Mallat and W. L. Hwang, "Singularity detection and processing with wavelets," *IEEE transactions on information theory*, vol. 38, no. 2, pp. 617–643, 2002.
- [40] M. Stephane, "A wavelet tour of signal processing," 1999.
- [41] Y. Wang and P. He, "Comparisons between fast algorithms for the continuous wavelet transform and applications in cosmology: The 1d case," *RAS Techniques and Instruments*, vol. 2, no. 1, pp. 307–323, 2023.
- [42] S.-H. Ieng, E. Lehtonen, and R. Benosman, "Complexity analysis of iterative basis transformations applied to event-based signals," *Frontiers in neuroscience*, vol. 12, p. 373, 2018.
- [43] A. Kumar, S. Saha, and R. Bhattacharya, "Improved wavelet transform based edge detection for wide band spectrum sensing in cognitive radio," in *2016 USNC-URSI Radio Science Meeting*. IEEE, 2016, pp. 21–22.
- [44] R. T. Kobayashi, L. Claudino, A. G. Hernandez, and T. Abrão, "Multiband spectrum sensing via edge detection using a wavelet approach."
- [45] Z. Tian and G. B. Giannakis, "Compressed sensing for wideband cognitive radios," in *2007 IEEE International conference on acoustics, speech and signal processing-ICASSP'07*, vol. 4. IEEE, 2007, pp. IV–1357.
- [46] J. A. Tropp and A. C. Gilbert, "Signal recovery from random measurements via orthogonal matching pursuit," *IEEE Transactions on information theory*, vol. 53, no. 12, pp. 4655–4666, 2007.
- [47] W. Dai and O. Milenkovic, "Subspace pursuit for compressive sensing signal reconstruction," *IEEE transactions on Information Theory*, vol. 55, no. 5, pp. 2230–2249, 2009.
- [48] R. Venkataramani and Y. Bresler, "Perfect reconstruction formulas and bounds on aliasing error in sub-nyquist nonuniform sampling of multiband signals," *IEEE Transactions on Information Theory*, vol. 46, no. 6, pp. 2173–2183, 2000.
- [49] D. Cabric, A. Tkachenko, and R. W. Brodersen, "Spectrum sensing measurements of pilot, energy, and collaborative detection," in *Milcom 2006-2006 IEEE military communications conference*. IEEE, 2006, pp. 1–7.
- [50] D. B. Cabric, "Cognitive radios: System design perspective," Ph.D. dissertation, University of California, Berkeley, 2007.
- [51] M. Zheng, L. Chen, W. Liang, H. Yu, and J. Wu, "Energy-efficiency maximization for cooperative spectrum sensing in cognitive sensor networks," *IEEE Transactions on Green Communications and Networking*, vol. 1, no. 1, pp. 29–39, 2016.
- [52] Q. Wu, B. K. Ng, and C.-T. Lam, "Energy-efficient cooperative spectrum sensing using machine learning algorithm," *Sensors*, vol. 22, no. 21, p. 8230, 2022.
- [53] W. Ejaz, G. A. Shah, N. u. Hasan, and H. S. Kim, "Energy and throughput efficient cooperative spectrum sensing in cognitive radio sensor networks," *Transactions on Emerging Telecommunications Technologies*, vol. 26, no. 7, pp. 1019–1030, 2015.
- [54] R. Deng, J. Chen, C. Yuen, P. Cheng, and Y. Sun, "Energy-efficient cooperative spectrum sensing by optimal scheduling in sensor-aided cognitive radio networks," *IEEE Transactions on Vehicular Technology*, vol. 61, no. 2, pp. 716–725, 2011.
- [55] S. Wang, Y. Wang, J. P. Coon, and A. Doufexi, "Energy-efficient spectrum sensing and access for cognitive radio networks," *IEEE transactions on vehicular technology*, vol. 61, no. 2, pp. 906–912, 2011.
- [56] X. Ding, T. Ni, Y. Zou, and G. Zhang, "Deep learning for satellites based spectrum sensing systems: A low computational complexity perspective," *IEEE Transactions on Vehicular Technology*, vol. 72, no. 1, pp. 1366–1371, 2022.
- [57] R. Mei and Z. Wang, "Deep learning-based wideband spectrum sensing: A low computational complexity approach," *IEEE Communications Letters*, 2023.
- [58] S. S. Alam, M. O. Mughal, L. Marcenaro, and C. S. Regazzoni, "Computationally efficient compressive sensing in wideband cognitive radios," in *2013 Seventh International Conference on Next Generation Mobile Apps, Services and Technologies*. IEEE, 2013, pp. 226–231.
- [59] O. Ronneberger, P. Fischer, and T. Brox, "U-net: Convolutional networks for biomedical image segmentation," in *Medical image computing and computer-assisted intervention—MICCAI 2015: 18th international con-*

ference, Munich, Germany, October 5-9, 2015, proceedings, part III 18. Springer, 2015, pp. 234–241.

- [60] N. Siddique, S. Paheding, C. P. Elkin, and V. Devabhaktuni, “U-net and its variants for medical image segmentation: A review of theory and applications,” *IEEE access*, vol. 9, pp. 82 031–82 057, 2021.
- [61] O. Oktay, J. Schlemper, L. L. Folgoc, M. Lee, M. Heinrich, K. Misawa, K. Mori, S. McDonagh, N. Y. Hammerla, B. Kainz *et al.*, “Attention u-net: Learning where to look for the pancreas,” *arXiv preprint arXiv:1804.03999*, 2018.
- [62] D.-H. Nguyen, T.-V. Nguyen, and T. Huynh-The, “Enhancing spectrum sensing for 5g and lte with improved u-net architecture,” in *2024 International Conference on Advanced Technologies for Communications (ATC)*. IEEE, 2024, pp. 167–172.
- [63] D. Uvaydov, M. Zhang, C. P. Robinson, S. D’Oro, T. Melodia, and F. Restuccia, “Stitching the spectrum: Semantic spectrum segmentation with wideband signal stitching,” in *IEEE INFOCOM 2024-IEEE Conference on Computer Communications*. IEEE, 2024, pp. 2219–2228.
- [64] K. Dakic, B. Al Homssi, and A. Al-Hourani, “Spiking-unet: Spiking neural networks for spectrum occupancy monitoring,” in *2024 IEEE Wireless Communications and Networking Conference (WCNC)*. IEEE, 2024, pp. 1–6.
- [65] J.-H. Park, D.-H. Park, and H.-N. Kim, “Target detection using u-net for a dtv-based passive bistatic radar system,” in *2022 International Conference on Artificial Intelligence in Information and Communication (ICAIIIC)*. IEEE, 2022, pp. 176–178.
- [66] N. West, T. Roy, and T. O’Shea, “Wideband signal localization with spectral segmentation,” *arXiv preprint arXiv:2110.00583*, 2021.
- [67] L. M. Leemis, *Reliability: probabilistic models and statistical methods*. Prentice-Hall, Inc., 1995.



Sundeep Rangan (Fellow, IEEE) received the B.A.Sc. degree in electrical engineering from the University of Waterloo, Waterloo, ON, Canada, and the M.Sc. and Ph.D. degrees in electrical engineering from the University of California, Berkeley, Berkeley, CA, USA.

He has held Postdoctoral appointments with the University of Michigan, Ann Arbor, Ann Arbor, MI, USA, and Bell Labs. In 2000, he co-founded (with four others) Flarion Technologies, a spin-off of Bell Labs, that developed Flash OFDM, the first cellular OFDM data system and pre-cursor to 4G cellular systems including LTE and WiMAX. In 2006, Flarion was acquired by Qualcomm Technologies. He was a Senior Director of Engineering at Qualcomm involved in OFDM infrastructure products. He joined New York University Tandon (formerly NYU Polytechnic), Brooklyn, NY, USA, in 2010, where he is currently a Professor of electrical and computer engineering. He is the Associate Director of NYU WIRELESS, Brooklyn, NY, an industry-academic research center on next-generation wireless systems.



Ali Rasteh received B.Sc. and M.Sc. degrees in electrical and computer engineering from Sharif University of Technology, Tehran, Iran, in 2015 and 2017, respectively. He is currently pursuing a Ph.D. degree in electrical and computer engineering at New York University, Brooklyn, NY, USA, where he is a member of the NYU Wireless research center. His major field of study is wireless communications.

He is currently a Research Assistant at NYU Wireless, where he works on wireless spectrum sensing, hardware development for communication systems, and AI/ML applications for 6G wireless. From 2015 to 2022, he held multiple positions at Sina Communication Systems Co., including Technical Lead and Hardware/Embedded Systems Developer, where he led development teams on advanced optical access and transport network hardware. He has also conducted part-time research with CNRS and the University of Toulouse, focusing on spiking neural networks. He has authored or co-authored several technical papers. His current research interests include 6G communication systems, efficient hardware design, and machine learning for wireless communications.

Mr. Rasteh is a member of NYU Wireless and the NYU Center for Advanced Technology in Telecommunications (CATT). He has been awarded full scholarships for his doctoral studies at New York University. He has contributed to numerous high-impact academic and industrial projects in communication technologies.